Journal of Physical Chemistry
Submission Window August 1 – September 30, 2017
W. Lester S. Andrews Festschrift
Submitted September 29, 2017
Revised November 15, 2017

Bond Dissociation Energies of Tungsten Molecules: WC, WSi, WS, WSe, and WCl [†]

Andrew Sevy, Robert F. Huffaker, and Michael D. Morse[*]
Department of Chemistry
University of Utah
Salt Lake City, UT 84112

[†]Submitted as part of the "W. Lester S. Andrews Festschrift"
[*] Corresponding author. E-mail: morse@chem.utah.edu
FAX: (801)-581-8433

ABSTRACT:

Resonant two-photon ionization spectroscopy has been used to locate predissociation thresholds in WC, WSi, WS, WSe, and WCl, allowing bond dissociation energies to be measured for these species. Because of the high degree of vibronic congestion in the observed spectra, it is thought that the molecules dissociate as soon as the lowest separated atom limit is exceeded. From the observed predissociation thresholds, dissociation energies are assigned as D_0(WC) = 5.289(8) eV, D_0(WSi) = 3.103(10) eV, D_0(WS) = 4.935(3) eV, D_0(WSe) = 4.333(6) eV, and D_0(WCl) = 3.818(6) eV. These results are combined with other data to obtain the ionization energy, IE(WC) = 8.39(9) eV, and the anionic bond dissociation energies of $D_0(W\text{-}C^-)$ = 6.181(17) eV, $D_0(W^-\text{-}C)$ = 7.363(19) eV, $D_0(W\text{-}Si^-) \leq$ 3.44(4) eV, and $D_0(W^-\text{-}Si) \leq$ 4.01(4) eV. Combination of the D_0(WX) values with atomic enthalpies of formation also provides $\Delta_f H^\circ_{0K}$ values for the gaseous WX molecules. Computational results are also provided, which shed some light on the electronic structure of these molecules.

I. INTRODUCTION

The chemical bond is fundamental to all of chemistry, and particularly to chemical enterprise, which seeks to manipulate materials by breaking existing chemical bonds and forming new ones, thereby converting readily available reactants to desired products. These processes are controlled by the thermochemistry of the individual reactions, which ultimately are governed by the energies of the chemical bonds involved. Accordingly, one of the most fundamental aspects of the chemical bond is the energy that is released when a bond is formed or which is absorbed when a bond is broken – the bond dissociation energy (BDE).

In a series of recent publications,[1-4] this group has demonstrated that the high density of electronic states that is present in many diatomic transition metal molecules provides an efficient pathway for dissociation as soon as the BDE is exceeded in energy. We have previously observed abrupt predissociation thresholds in diatomic transition metal molecules such as NiPt,[5] AlNi,[6] Co_2^+,[7] and many others,[8-11] but only recently have we attempted to extend these observations to transition metals bonded to nonmetals and metalloids. In our most recent work, sharp predissociation thresholds in VC, VN, VS, FeC, FeS, FeSe, NiC, NiS, NiSe, MSe (M=Ti, Zr, Hf, V, Nb, Ta), and MSi (M=Ti, Zr, Hf, V, Nb, Ta) have been reported.[1-4] The predissociation thresholds that have been observed provide, at a minimum, upper bounds to the BDEs of the respective molecules. In systems with a sufficiently high density of electronic states, however, we have argued that predissociation sets in as soon as the lowest separated atom limit is exceeded.[8, 9] If rapid predissociation sets in at the thermochemical threshold, the measured predissociation threshold provides the BDE of the molecule.

In early work on V_2, the predissociation threshold was found at 22 201 ± 1 cm^{-1}, [8, 9] while a predissociation threshold in the V_2^+ cation was found at 25 326 ± 15 cm^{-1}.[12] In independent experiments, the ionization energies IE(V) = 54 411.67 ± 0.17 cm^{-1} and IE(V_2) = 51 271.14 ± 0.50 cm^{-1} were also measured.[13, 14] These four quantities are related through the thermochemical cycle

$$D_0(V_2) + IE(V) - IE(V_2) - D_0(V_2^+) = 0. \quad (1.1)$$

Evaluating the right hand side of equation (1.1) provides a value of 15.5 ± 15 cm^{-1}, showing that the predissociation-based values of $D_0(V_2)$ and $D_0(V_2^+)$ satisfy the thermochemical cycle to high accuracy. Because no barrier is expected to prevent dissociation at the thermochemical threshold in V_2^+, the satisfaction of this thermochemical cycle implies that the neutral V_2 molecule also predissociates at the thermochemical threshold, proving that $D_0(V_2)$ = 22 201 cm^{-1}, to 15 cm^{-1} accuracy or better. Currently, V_2 provides the only example of predissociation-based bond dissociation energies where all four values are known to such accuracy; therefore, this is the only example where the validity of the predissociation-based measurements may be considered proven. We have argued, however, that predissociation is highly likely to set in at the lowest separated atom limit in examples where a sharp predissociation threshold is observed in the spectrum of a molecule that has a high density of states, particularly when a large number of states correlate to the ground separated atom limit.[8, 9]

We are currently applying this method to measure BDEs of a number of diatomic transition metal-main group molecules, with the goal of developing a significant database of well-determined BDEs for transition metal (and ultimately for lanthanide and actinide) systems. Such a database will allow periodic trends to be better understood, and will provide

benchmarks that may be used to test computational methods. This is particularly important for the *d*- and *f*-block metals, where data of high precision is currently limited and computational methods face significant challenges.[15-17]

In the present investigation, we focus on chemical bonding between the tungsten atom and the main group elements C, Si, S, Se, and Cl. The high nuclear charge of W causes relativistic effects, including spin-orbit interaction, to be significant while the open 5*d*-subshell makes electron correlation effects quite substantial as well. Thus, the BDEs of WC, WSi, WS, WSe, and WCl reported here provide serious challenges for the computational chemist. It is our hope that the BDEs we report for these molecules can be used to hone computational methods to greater accuracy.

II. EXPERIMENTAL SECTION

The predissociation thresholds of WC, WSi, WS, WSe, and WCl were measured using the resonant two-photon ionization spectrometer that was used in other recent studies from this group, including measurements of the BDEs of VC, VN, VS, MSe and MSi (M= Ti, Zr, Hf, V, Nb, Ta).[1, 2, 4] A tungsten metal disk was ablated using the 3rd harmonic output of a Nd:YAG laser (355 nm, ~7 mJ per pulse incident on the target), and the resulting products of ablation were carried down a 0.5 cm diameter channel, 1.3 cm in length, using a pulse of helium carrier gas seeded with a reaction gas (4% CH_4, 0.13% SiH_4, 0.67% H_2S, 0.1% H_2Se, or <0.1% HCl). Upon exiting the reaction channel, the carrier gas and reaction products were supersonically expanded into vacuum (10^{-5} Torr).

In the cases of CH_4, SiH_4, and H_2S, the reactant gases were purchased and further diluted in helium to obtain appropriate mixtures. Hydrogen selenide was synthesized as

outlined in our previous publication.[2] In one of our H_2Se syntheses, a rather large amount of HCl was accidentally condensed with the H_2Se product, leading to a contaminated gas mixture. As a result, experiments conducted with that carrier gas mixture produced a substantial amount of WCl. This fortuitous accident allowed us to measure the BDE of WCl along with that of WSe. Because these molecules are detected mass-specifically, it was straightforward to measure the BDE of WCl independently of the BDE of WSe.

The supersonic expansion was skimmed to form a molecular beam 1 cm in diameter, after which it entered the Wiley-McLaren ion source of a reflectron time-of-flight mass spectrometer.[18, 19] There it was interrogated by a pulse of tunable radiation produced by an optical parametric oscillator (OPO) laser that was counterpropagated along the molecular beam. Radiation produced by a KrF (248 nm, 5.00 eV) excimer laser was directed across the molecular beam about 20-30 ns after the OPO laser was fired, and ions produced by absorption of either two photons of OPO radiation or by one photon of OPO radiation and one KrF excimer photon were detected in the time-of-flight mass spectrometer. The KrF excimer laser intensity was reduced using poor quality fused silica plates so that the ion signal produced by two-photon processes involving only the KrF wavelength was minimized.

The instrument was operated at a 10 Hz repetition rate, and 30 shots were averaged for each wavelength point. Multiple mass-to-charge species were monitored in each scan, allowing spectra of several species to be simultaneously recorded. Atomic transitions were used to calibrate the wavenumber axis, using the NIST tables of atomic energy levels.[20] For WSi, the W atomic transitions proved difficult to identify, so the scan was repeated using a titanium sample and the Ti atomic transitions were used for calibration. For WC, WS, WSe,

and WCl, tungsten atomic transitions were readily identified and calibration was straightforward.

III. COMPUTATIONAL METHODS

The Gaussian 09 software suite was employed for all computations.[21] Using the LANL2DZ basis set,[22] calculations were performed in the C_{2v} point group using the B3LYP density functional method.[23, 24] The LANL2DZ basis set uses an effective core potential that makes the computations much more tractable, and includes mass-velocity and Darwin relativistic effects on the core electrons. Unrestricted geometry optimization and frequency calculations were performed to attempt to determine the ground state of each WX molecule. All calculations were performed using a super-fine grid in order to insure that the integrations were sufficiently accurate. Alternative configurations were examined by altering the orbital occupations and running the calculation again. Singlet, triplet, and quintet spin states were considered for WC, WSi, WS, and WSe; doublet, quartet, and sextet states were computed for WCl. For each calculated multiplicity, the electron configuration was assigned based on the apparent orbital symmetry, and possible term symbols were deduced. Finally, separate calculations on the ground state energies of the tungsten and ligand atoms were performed, in order to obtain computational estimates of the BDE by difference.

To estimate the effects of spin-orbit interaction on the computed BDE, the spin-orbit stabilization of the separated atoms was computed as the difference between the degeneracy-weighted average of the spin-orbit levels of the ground atomic term, and the lowest atomic spin-orbit level. The spin-orbit stabilization energy of the lowest level of the molecule was calculated using methods described by Lefebvre-Brion and Field for the states that are

considered good candidates for the ground state.[25] These methods are described in greater detail for the individual molecules in Section IV.C below.

IV. RESULTS

A. Experimental Results

1. WC

Figure 1 displays the resonant two-photon ionization (R2PI) spectrum of WC, recorded over the range 39,500 – 44,500 cm^{-1}. A strong, structured but continuous, R2PI signal is observed, followed by a sharp drop to baseline at 42,655 ± 65 cm^{-1} (5.289 ± 0.008 eV). The continuous absorption spectrum, combined with the abrupt drop to baseline, suggests that predissociation sets in at the lowest separated atom limit, W $5d^4 6s^2$, $^5D_{0g}$ + C $2s^2 2p^2$, $^3P_{0g}$. A problem with this ground separated atom limit, however, is that the combination of two J=0 atoms generates only one molecular state, with $\Omega = 0^+$.[26] Additional potential curves with $\Omega = 0^-$ and 1 arise from the W $5d^4 6s^2$, $^5D_{0g}$ + C $2s^2 2p^2$, $^3P_{1g}$ limit,[26] which lies 16.40 cm^{-1} higher in energy.[20] Finally, the separated atom limit of W $5d^4 6s^2$, $^5D_{0g}$ + C $2s^2 2p^2$, $^3P_{2g}$, lying at 43.40 cm^{-1},[20] generates three molecular states with $\Omega = 0^+$, 1, and 2.[26] The next separated atom limit above these states involves excitation of the W atom to $5d^4 6s^2$, $^5D_{1g}$ and lies at 1670.29 cm^{-1}.[20] In our spectra, we find no evidence of a second dissociation threshold 1670 cm^{-1} higher (or lower) than the observed sharp threshold, so we are convinced that the observed predissociation threshold corresponds to dissociation to the lowest group of separated atom asymptotes, W $5d^4\ 6s^2$, $^5D_{0g}$ + C $2s^2\ 2p^2$, $^3P_{0,\,1,\,2g}$.

The ground state of WC is known to be $X_1\ ^3\Delta_1$, arising from the $1\sigma^2\ 2\sigma^2\ 1\pi^4\ 3\sigma^1\ 1\delta^1$ configuration.[27-30] Allowed optical transitions from this state can populate levels with

$\Omega' = 0^+$, 0^-, 1, and 2, all of which can dissociate to the lowest three separated atom limits while preserving the value of Ω. Thus, there is no symmetry-based restriction on dissociation to these limits, which can occur through curve hopping induced by spin-orbit interaction and nonadiabatic coupling. States with $\Omega' = 1$ or 2 that are of *e* parity are also coupled to the $\Omega' = 0^+$ state that derives from the ground separated atom limit through the **L**-uncoupling and **S**-uncoupling operators,[25] providing a mechanism for their dissociation at the lowest separated atom asymptote. States reached by optical excitation from the ground state that have $\Omega' = 0^-$, 1 or 2, but which have *f* parity, however, cannot dissociate to ground state atoms because the *e/f* parity must be conserved, unless hyperfine perturbations are present.[25] Both nuclei of the $^{182}W^{12}C$ isotopologue displayed in Figure 1, however, lack nuclear spin (I=0), so hyperfine perturbations are absent. Thus, *e/f* parity must be conserved in the dissociation process. Excited states of *f* parity cannot dissociate until the first excited separated atom limit, W $5d^4\ 6s^2$, $^5D_{0g}$ + C $2s^2\ 2p^2$, $^3P_{1g}$, is reached, 16.40 cm^{-1} above ground state atoms.[20] This small excitation energy is similar to the line width of the laser used to record the spectrum, so we are unable to discern whether dissociation occurs with two distinct thresholds that are separated by this interval.

In the absence of experimental evidence allowing us to identify the separated atom asymptotes that are associated with the sharp predissociation threshold, we have chosen simply to increase the assigned error limit for the BDE of WC to encompass all three asymptotes, W $5d^4\ 6s^2$, $^5D_{0g}$ + C $2s^2\ 2p^2$, $^3P_{0,\,1,\,2g}$. The overall separation between these limits is 43.40 cm^{-1}, an amount that falls well within the assigned error of ±65 cm^{-1}. Therefore, we report the BDE of WC as $D_0(WC)$ = 42,655(65) cm^{-1}, or 5.289(8) eV.

2. WSi

Figure 2 displays the R2PI spectrum of WSi, recorded over the range from 23,500 to 26,600 cm^{-1}. Again, an abrupt predissociation threshold is observed in a congested and quasi-continuous electronic spectrum, at 25,107(25) cm^{-1}. It is tempting to assign this sharp predissociation threshold as the BDE of the WSi molecule, but the level structure at the separated atom limit in WSi is identical to that of WC, just with a larger spin-orbit splitting. Therefore, the same issues that complicate the situation in WC are also present in WSi.

The lowest three separated atom limits in WSi are W $5d^4 6s^2$, $^5D_{0g}$ + Si $3s^2\ 3p^2$, $^3P_{0,\,1,\,2g}$, lying at 0, 77.1, and 223.2 cm^{-1}, respectively.[20] The ground state of WSi is experimentally unknown, and computational studies have not resolved the question.[31-33] Regardless of the details of the ground and excited electronic states, however, that fact remains that excited states of *f* parity cannot dissociate at the ground separated atom limit, which only generates states of *e* parity. Thus, we expect to see two dissociation thresholds separated by the spin-orbit excitation energy of Si, 77.1 cm^{-1}.

Figure 3 displays an expanded view of the WSi spectrum in the region of the predissociation threshold. The final drop to baseline follows a nearly linear drop, and the same linear drop has been applied to a feature that appears in the spectrum about 77 cm^{-1} to lower energy. If we extrapolate these two lines to the baseline, the intersections with baseline occur at 25,120.1 and 25,042.6 cm^{-1}, giving a separation of 77.5 cm^{-1}. This agrees with the expected separation of 77.1 cm^{-1} better than should be expected given the linewidth of the OPO laser, which is about 10 cm^{-1} based on the weaker Ti atomic transitions (which are not power broadened) near 24,914 and 24,967 cm^{-1}.

It appears that the BDE of WSi is given by the lower energy drop to baseline. However, to account for possible errors of interpretation, we think it prudent to apply a conservative error limit of ±80 cm^{-1} to this value, in order to encompass both dissociation thresholds. Accordingly, we assign $D_0(WSi) = 25{,}030(80)$ cm^{-1}, or 3.103(10) eV.

3. WS

Figure 4 displays the R2PI spectrum of WS, over the range 35,000 - 43,000 cm^{-1}. Shown in blue is the signal arising from the absorption of one tunable OPO laser photon, followed by ionization by absorption of a KrF laser photon (248 nm, 5.00 eV) after a delay of about 30 ns. A clean drop to baseline is observed at 39,800 ± 25 cm^{-1}. We assign this as the BDE of WS, providing $D_0(WS) = 4.935(3)$ eV. Unlike the situation for WC and WSi, the ground separated atom limit, W $5d^4\ 6s^2$, $^5D_{0g}$ + S $3s^2\ 3p^4$, $^3P_{2g}$, generates molecular states with $\Omega = 0^+$, 1, and 2. Both *e* and *f* parity states can dissociate at this limit, because although $\Omega = 0^+$ only generates levels of *e* parity, the Ω = 1 and 2 potential curves support levels of both *e* and *f* parity. The only type of state that is rigorously unable to predissociate at this limit is an excited level of *f* parity with J = 0. While J=0*f* states may be populated when WS absorbs a photon, the relatively warm rotational temperature obtained when expanding from a 5 mm orifice (T > 20 K) guarantees that these will be a small fraction of the population. For this reason, the molecule exhibits a sharp dissociation threshold with no persistent signal above 39,800 cm^{-1} when ionized after a 30 ns delay.

When investigating the predissociation threshold of WS, it was readily apparent that the molecule can be ionized by absorption of either two OPO laser photons, or by one OPO photon and one KrF photon. Because the OPO laser is fired roughly 30 ns before the KrF laser, these two ionization processes lead to separate peaks in the time-of-flight mass

spectrum, with the peak that appears earlier in time resulting from the OPO + OPO ionization process. The second peak results from the OPO + KrF ionization process. In Figure 4 we display the spectra observed when each peak is monitored. The two signals differ because in the OPO + OPO case, excited states are detected if they can be ionized within 5 ns; in the OPO + KrF case, only states that live for 30 ns are detected. Figure 4 shows a clean baseline above 39,800 cm^{-1} in the OPO + KrF delayed ionization spectrum (in blue), but a weak ion signal persists in the prompt ionization spectrum (displayed in black) until a second dissociation threshold is reached near 41,455 cm^{-1}. The states that are observed above 39,800 cm^{-1} in the prompt ionization spectrum are states with a short lifetime ($\tau < 30$ ns), but which can still be ionized within the 5 ns OPO laser pulse. Based on the intensity of this residual signal, only a small fraction of the states excited above 39,800 cm^{-1} are able to survive long enough to be ionized, even within the 5 ns timeframe. The low intensity of this residual signal shows that states lying above 39,800 cm^{-1} dissociate rapidly, probably in less than 1 ns.

Although the higher energy dissociation threshold is somewhat ill-defined, it is located at approximately 41,455(25) cm^{-1}. The difference between the two thresholds, combining the errors, is then 1655(35) cm^{-1}. This separation corresponds closely to the energy of the first excited spin-orbit level of tungsten, $^5D_{1g}$, lying at 1670.29 cm^{-1}.[20] It seems that the predissociation rate increases markedly when the W $5d^4 6s^2$, $^5D_{1g}$ + S $3s^2 3p^4$, $^3P_{0g}$ separated atom limit is exceeded. Excited states lying above this limit decay too quickly to be detected, even in the OPO + OPO ionization process.

Finally, it is worth noting that in all of these studies, the ion signal in the atomic channel is much greater than that of the molecule of interest. Generally, the atomic signals

are so strong that on resonance they saturate our detection system. Clean atomic spectra are more readily obtained for minor isotopes that saturate the detector less readily, such as ^{180}W (0.13% natural abundance), as shown in Figure 4. Even in that case, the atomic spectra are plotted on a greatly reduced scale compared to the molecular spectra. Another option, which we frequently employ, is to collect calibration scans over atomic transitions separately, under conditions that are optimized for clean, well-resolved atomic features. Under conditions of high OPO intensity (as was used for the OPO + OPO scan displayed in black in Figure 4), the intense atomic transitions are also observed as depletions of the WS ion signal. We believe this occurs because so many atomic ions are produced on resonance that Coulomb repulsions cause the ion cloud to expand as it traverses the drift tube, preventing most ions of a given species from reaching the detector. The result is depletion of all ion signals except for the atomic ion signal, which completely dominates the mass spectrum. An example is the strong atomic transition near 38,400 cm^{-1} in the $^{180}W^+$ mass channel, which is readily apparent as a depletion in the WS^+ signal, particularly in the black OPO + OPO spectrum. Artificial drops in molecular signal arising from this effect are evident in all of the spectra collected in this work, as well as in previous work.[1-4]

4. WSe

Figure 5 displays a scan over the 32,000-40,000 cm^{-1} range in the R2PI spectrum of WSe, with the spectrum of atomic W displayed below. As in the WS example, the molecular signal reflects the intense atomic transitions as depletions in signal, mirroring the atomic spectrum. The drop to baseline occurs at 34,947 ± 50 cm^{-1}. Like sulfur, selenium has a $^3P_{2g}$ ground level, which in combination with the $^5D_{0g}$ level of tungsten, generates $\Omega = 0^+$, 1, and 2 electronic states. Similarly to WS, the only states of WSe that cannot dissociate at the

ground separated atom limit are excited states with J = 0*f*. The first excited spin-orbit asymptote for the system is the W $5d^4\ 6s^2$, $^5D_{1g}$ + Se $4s^2\ 4p^4$, $^3P_{0g}$ level at 1670.3 cm^{-1}; the next excited atomic asymptote is W $5d^4\ 6s^2$, $^5D_{0g}$ + Se $4s^2\ 4p^4$, $^3P_{1g}$ level 1989.5 cm^{-1}.[20] The spectrum shows no evidence of a second predissociation threshold at either of these energies. On this basis, we assign the bond dissociation energy of WSe as 34,947(50) cm^{-1}, or 4.333(6) eV.

5. WCl

Figure 6 displays a scan over the predissociation threshold of WCl in the 28,500-35,500 cm^{-1} range. A drop to baseline is clearly observed at 30,796 ± 50 cm^{-1}, although weak vibronic bands persist to much higher wavenumbers. The ground separated atom limit for this system is W $5d^4 6s^2$, $^5D_{0g}$ + Cl $3s^2 3p^5$, $^2P_{3/2u}$, which generates two potential energy curves: Ω = 1/2 and Ω = 3/2. Both curves have both *e* and *f* components, so predissociation at this limit is possible for all excited states with Ω′ = 1/2 or 3/2, via Ω-preserving curve hopping processes. States with higher values of Ω′ can also dissociate at this limit via **L**- and **S**-uncoupling perturbations,[25] which destroy Ω as a good quantum number. Quantum chemical computations (see below) strongly suggest that the ground term of WCl is of $^6\Sigma^+$ symmetry, which possesses Ω = 1/2, 3/2, and 5/2. Thus, excited states with Ω′ as large as 7/2 may be reached by allowed electric dipole transitions. Such states would have to undergo two Ω-changing interactions in order to permit dissociation to ground state atoms on the Ω=3/2 potential energy surface. We suggest that the states that are observed above the sharp predissociation threshold correspond to Ω′ = 7/2 states that dissociate less efficiently because of the need to undergo two Ω-changing interactions. Some Ω′ = 5/2 states may also

contribute; these require only one Ω-changing interaction to be coupled to the Ω=3/2 curve that arises from ground state atoms.

The first excited separated atom limit in the WCl system is W, $5d^4\ 6s^2\ ^5D_{0g}$ + Cl $3s^2 3p^5$, $^2P_{1/2g}$, at 882.4 cm^{-1}.[20] There is no evidence of a second dissociation threshold at this separation from the observed threshold, so it appears that the vast majority of the electronic states reached are able to dissociate to ground state atoms. Therefore, we assign the bond dissociation energy of WCl as 30,796(50) cm^{-1}, or D_0(WCl) = 3.818(6) eV.

B. Computational Results

For all five molecules considered here, the valence molecular orbitals derive from the 5*d* and 6*s* orbitals of W and the n*s* and n*p* orbitals of the ligand, leading to four orbitals of σ symmetry (numbered here as the 1σ through 4σ orbitals), two pairs of π orbitals (1π and 2π), and one pair of δ orbitals (1δ). A qualitative depiction of the molecular orbitals, using orbitals obtained for α spins in the calculation of the $^3\Sigma^-$ state of WS is displayed in Figure 7. For WC and WSi, 10 valence electrons are distributed in these orbitals; for WS and WSe, there are 12 valence electrons; and for WCl, there are 13 valence electrons.

In all five molecules, the 1σ orbital is fully occupied in the low-lying states, and is composed mainly of ligand n*s* character. Although the order of the orbitals varies in the set of WX molecules, and in the electronic configuration examined, one of the 2σ/3σ orbitals is a bonding orbital consisting mainly of W 5*d*σ and ligand n*p*σ character. This is the 2σ orbital in WS. The other (3σ in WS) is primarily W 6*s* in character, with an admixture of 5*d*σ character so that it resembles a donut that places electron density off the molecular axis, making it primarily nonbonding in character. This 6*s*-based σ orbital is lower in energy than might be expected because of the relativistic stabilization of the 6*s* orbital, which also causes

the W atom to have a ground configuration of $5d^4 6s^2$, rather than the $d^5 s^1$ ground configuration found in isovalent Cr and Mo. The 1π orbital is a bonding combination of the W 5*d*π and nonmetal n*p*π orbitals, with greater contributions from the nonmetal n*p*π orbitals, particularly for the more electronegative ligands. Close in energy to the 3σ orbital is the nonbonding 1δ pair of orbitals, which are nearly pure W 5*d*δ in character. Above these lie the antibonding 2π orbitals, composed of W 5*d*π and ligand n*p*π character, with greater contributions from W 5*d*π, especially for the more electronegative ligands. Finally, at very high energy lies the 4σ antibonding orbital. This is empty in the low-lying states of all five WX molecules.

To try to identify the ground electronic states, we have calculated a number of different electronic configurations and terms for all five WX molecules. The results are provided in Table 1, where we have listed the states in order of increasing energy. Where possible, term symbols have been identified. In some cases, the configuration examined can generate multiple terms, as in the $1\sigma^2 1\pi^3 2\sigma^2 1\delta^1 3\sigma^2$ of WC, which generates both $^3\Pi$ and $^3\Phi$. In these cases, all of the possible terms are listed. In addition to the term energy, T_0, which is given as the energy of the v=0 level of the state in question, relative to the v=0 level of the ground state, we also report the dipole moment at the equilibrium position, the harmonic frequency (ω_e), the equilibrium bond length (r_e), and the bond dissociation energy ignoring spin-orbit corrections (D_0). Because the calculations were performed using the unrestricted B3LYP method for states with nonzero spin, the calculated states are not eigenfunctions of $\hat{S}^2$. The expectation values, $\langle \hat{S}^2 \rangle$, have been calculated and set equal to S(S+1), and the resulting equation has been solved for S, which is reported as <S> in the table. This is a useful diagnostic, as it should precisely equal 0.5 for doublet states, 1.0 for triplet states, 1.5

for quartet states, *etc.* When the discrepancy is significant, the spin-contaminated result should be considered less trustworthy.

1. WC

Of the five WX molecules reported here, WC is the only molecule for which the ground electronic state is experimentally known.[27-30, 34, 35] The ground state is $1\sigma^2 1\pi^4 2\sigma^2 1\delta^1 3\sigma^1$, $^3\Delta_1$, with an r_0 bond length of 1.7143 Å and a harmonic frequency of ω_e = 983(4) cm^{-1}.[27, 30] The ground state dipole moment is 3.90(4) D.[29] The molecule is of particular interest because the existence of a $^3\Delta_1$ ground state in a molecule containing a highly charged nucleus makes it an excellent candidate for the measurement of the dipole moment of the electron, a topic of intense interest in particle physics.[34, 35] The calculated values of the molecular constants show exceptionally good agreement for ω_e, a moderate disagreement (8.5%) in dipole moment, and an error of 0.022 Å in bond length. This is a reasonable level of agreement, overall. The calculated BDE of 4.90 eV, omitting spin-orbit corrections, is significantly less than the measured value of 5.289(8) eV. Spin-orbit corrections to D_0 for WC and the other molecules are considered in Section IV.C below.

In addition to the computational work presented here, WC has been previously investigated using the B3LYP functional with the LANL2DZ basis set for W (as we have done here), but with the 6-311++G(df) basis set for C.[36] The result predicts a ground term of $1\sigma^2 1\pi^4 2\sigma^2 1\delta^2$, $^3\Sigma^-$ with ω_e = 1009 cm^{-1}, r_e = 1.704 Å, and a BDE of D_0(WC) = 5.16 eV, without any corrections for spin-orbit effects.[36] While this calculated ground state is incorrect, the study does not report the energies of low-lying excited states, so it is possible that the $^3\Delta$ term lies very close in energy using this methodology.

A far more detailed study of the electronic states of WC has been undertaken using the complete active space multiconfiguration self-consistent field-configuration interaction (CASMCSCF-CI) method, followed by relativistic configuration interaction (RCI) methods to include spin-orbit interaction and other relativistic effects.[37] The calculation finds the ground state to be $1\sigma^2 1\pi^4 2\sigma^2 1\delta^1 3\sigma^1$, $^3\Delta_1$, in agreement with experiment, and predicts a spin-orbit corrected BDE of 5.8 eV, 0.5 eV higher than found in our experiment. The calculated bond length (r_e), vibrational frequency (ω_e), and dipole moment (μ_e) of 1.727 Å, 977.5 cm^{-1}, and 4.211 D are in good agreement with the experimental values.

2. WSi

Our computations suggest a ground electronic state of $1\sigma^2 1\pi^4 2\sigma^2 1\delta^1 3\sigma^1$, $^3\Delta$ for WSi, exactly as found for the isovalent WC molecule. The calculated BDE is 2.77 eV, omitting spin-orbit corrections, which is 0.33 eV smaller than the measured value of 3.103(10) eV. The $1\sigma^2 1\pi^4 2\sigma^1 1\delta^2 3\sigma^1$, $^5\Sigma^-$ state is computed to lie 0.38 eV higher in energy. These results differ from a previous investigation employing the B3LYP method with the LANL2DZ basis set for W and the 6-311++G(df) basis for Si, which finds a $1\sigma^2 2\sigma^2 1\pi^3 1\delta^2 3\sigma^1$, $^5\Pi$ ground state with a spin-orbit uncorrected bond energy of D_0(WSi) = 2.96 eV.[32] In that work, a triplet state of undefined nature was found to lie 0.16 eV higher in energy.

A more detailed computation of the low-lying states of WSi was subsequently undertaken, using the unrestricted B3LYP method and two different basis sets (LANL2DZ for both W and Si, and LANL2DZ for W, 6-311++G(3df, 3pd) for Si).[33] An unrestricted CCSD(T) calculation was also undertaken with these same two basis sets in the same study. For both the B3LYP and CCSD(T) calculations, the better basis set (LANL2DZ for W;

6-311++G(3df, 3pd) for Si) identified the ground state as a quintet, which was assigned as $1\sigma^2 1\pi^4 2\sigma^1 1\delta^2 3\sigma^1$, $^5\Sigma^-$. The computed bond dissociation energy was not reported.

These results identify three different candidates for the WSi ground term: $1\sigma^2 1\pi^4 2\sigma^2 1\delta^1 3\sigma^1$, $^3\Delta$; $1\sigma^2 1\pi^4 2\sigma^1 1\delta^2 3\sigma^1$, $^5\Sigma^-$; and $1\sigma^2 2\sigma^2 1\pi^3 1\delta^2 3\sigma^1$, $^5\Pi$. At this time, the computational results are not sufficiently clear to allow assignment of one of these as the unambiguous ground state. In this respect, WSi is reminiscent of our findings on the group 4 and 5 metal silicides, TiSi, ZrSi, HfSi, VSi, NbSi and TaSi,[4] which were also problematic for the computational determination of the ground electronic state. We anticipate that species with comparatively weak bond energies and for which the ground separated atom limit generates many terms will continue to be problematic in this regard. When there are a large number of states packed into a narrow energy range, it will generally be difficult to computationally determine which is the ground state.

3. WS and WSe

The electronic structures of WS and WSe are calculated to be similar, with two computed low-lying states as strong candidates for the ground state: $1\sigma^2 1\pi^4 2\sigma^2 1\delta^2 3\sigma^2$, $^3\Sigma^-$ and $1\sigma^2 1\pi^4 2\sigma^2 1\delta^2 3\sigma^1 2\pi^1$, $^5\Pi$. Here, comparisons to known isovalent species are relevant. The ground states of CrO,[38] CrS,[39, 40] and MoO[41] are experimentally known to be $1\sigma^2 1\pi^4 2\sigma^2 1\delta^2 3\sigma^1 2\pi^1$, $^5\Pi$, and the ground state of MoS is calculated to be the same.[42, 43] In contrast, the ground state of WO is $1\sigma^2 1\pi^4 2\sigma^2 1\delta^2 3\sigma^2$, $^3\Sigma^-$.[44, 45] To our knowledge, neither WS nor WSe have been investigated prior to this work. The discrepancy between the Cr and Mo chalcogenides and WO arises because of relativistic stabilization of the 6*s* orbital of W, which is the primary contributor to the 3σ molecular orbital. While this 3σ relativistic stabilization will persist in both WS and WSe, the strength of π-bonding is expected to

weaken as one moves down the chalcogenide series. The $^5\Pi$ term has an advantage of more favorable exchange interactions, compared to the $^3\Sigma^-$ term, but this comes at the cost of placing an electron in the antibonding 2π orbital, weakening the π bonding in the molecule. In WO, π-bonding is quite important; accordingly, the $^5\Pi$ term has been calculated to lie 9463 cm^{-1} (1.17 eV) above the $^3\Sigma^-$ ground term.[45] In WS, π-bonding is expected to be significantly weaker due to reduced $d\pi$-$p\pi$ overlap, so placement of an electron in the 2π orbital is not as disfavored as in WO. Our results still predict a $^3\Sigma^-$ ground term, but the $^5\Pi$ term is calculated to lie only 0.09 eV higher. This situation reverses in WSe, where the $^5\Pi$ term is calculated to be the ground term, with the $^3\Sigma^-$ term lying only 0.05 eV higher. These differences are not sufficient to identify the ground term in either WS or WSe, but serve to demonstrate how the energetics of these states are expected to change as one moves down the series of tungsten chalcogenides.

The computed BDEs, ignoring spin-orbit corrections, are D_0 (WS) = 4.10 eV and D_0(WSe) = 3.59 eV, substantially smaller than the measured values of 4.935(3) and 4.333(6) eV, respectively. Nevertheless, the calculation predicts a weakening of the WX bond by 0.51 eV in moving from WS to WSe, as compared to the measured weakening of 0.60 eV. The magnitude of the absolute error in these two examples demonstrates that the computational method and/or basis set is insufficient for the accurate calculation of bond energies in these systems.

4. WCl

Of all the molecules computationally investigated, WCl offers the cleanest determination of the ground state configuration and term, a high-spin $^6\Sigma^+$ state deriving from the $1\sigma^2 1\pi^4 2\sigma^2 1\delta^2 3\sigma^1 2\pi^2$ configuration. The next computed state is $1\sigma^2 1\pi^4 2\sigma^2 1\delta^1 3\sigma^2 2\pi^2$,

$^4\Delta$, lying 0.84 eV higher in energy. This result is consistent with the known ground states of the congeners CrF,[46, 47] and CrCl,[48, 49] and the calculated ground states of MoF, MoCl, MoBr, MoI,[50] and WF.[51] In these diatomics, the highly electronegative character of the halogen leads to a wide separation between the halogen based 1σ, 2σ, and 1π orbitals (which are primarily halogen n*s*, n*p*σ, and n*p*π in character) and the metal based 1δ, 3σ, and 2π orbitals, which are primarily W 5*d*δ, 6*s*σ, and 5*d*π in character. The large separation leads to a reduced orbital interaction between the two centers, making the WCl molecule more ionic than the other species considered here. As a result, the metal-based orbitals are close in energy, leading to the formation of a high-spin $1\sigma^2 1\pi^4 2\sigma^2 1\delta^2 3\sigma^1 2\pi^2$, $^6\Sigma^+$ ground state in which the partially occupied orbitals are dominated by tungsten atomic character.

The calculated bond dissociation energy, omitting spin-orbit corrections, is 3.80 eV. This is quite close to the measured value of 3.818(6) eV.

C. Spin-orbit corrections to computed bond dissociation energies

Although the LANL2DZ basis set includes mass-velocity and Darwin relativistic effects on the core electrons, it does not include spin-orbit effects. These have the effect of lowering the separated atom limits, as the terms separate out into spin-orbit levels. Likewise, the molecular ground state also separates into Ω-levels, leading to a spin-orbit stabilization. To investigate these effects, we have estimated the spin-orbit stabilization energy at the separated atom limit and for the various molecular states.

1. Corrections at the atomic limit

To calculate the spin-orbit stabilization at the separated atom limit, we calculate the degeneracy-weighted average of the atomic energy levels, and note the amount that the ground level lies below the average. Using the NIST atomic energy levels, in which the

ground level lies at 0 cm^{-1},[20] this provides a spin-orbit stabilization energy of each atom given by

$$\Delta E^{SO}(\text{atom}) = -\left[\sum_J (2J+1)E_J\right]/\left[\sum_J (2J+1)\right]. \quad (4.1)$$

For W, C, Si, S, Se, and Cl, these values are -0.553, -0.003, -0.015, -0.020, -0.096, and -0.024 eV, respectively. Of course, the spin-orbit stabilization energy of a given separated atom limit is just the sum of the stabilization energies of the two individual atoms. Accordingly, the separated atom limits W + C, W + Si, W + S, W + Se, and W + Cl are stabilized by -0.556, -0.568, -0.572, -0.648, and -0.577 eV, respectively.

2. First-order corrections for molecular states

For states with $\Lambda \neq 0$, the spin-orbit stabilization of the lowest Ω level may be estimated by first order perturbation theory.[25] First, one must set up a configuration for the partially occupied orbitals that reproduces the expected ground level of the term. This is best illustrated by example. The $1\sigma^2\ 1\pi^4\ 2\sigma^2\ 1\delta^1\ 3\sigma^1$, $^3\Delta$ term of WC, for example, generates spin-orbit levels with Ω = 1, 2, or 3. The orbital responsible for the spin-orbit splitting, 1δ, is less than half-full, so the term is regular with a $^3\Delta_1$ ground level, as is experimentally observed. Considering only the partially filled orbitals, the wavefunction for this level may be written as $|\Psi\rangle = |1\delta_{+2}(1)\beta(1)3\sigma(2)\beta(2)\rangle$. It may be readily verified that this wavefunction reproduces the values S = 1, Λ = +2, Ω = +1 ($^3\Delta_1$).

Next, the first order correction to the energy of the state may be computed as

$$E^{(1)} = \langle\Psi|\hat{H}^{SO}|\Psi\rangle = \langle\Psi|\sum \hat{\zeta}(r_{iI})\hat{\boldsymbol{\ell}}_{iI}\cdot\hat{\mathbf{s}}_i|\Psi\rangle, \quad (4.2)$$

where the summation runs over all electrons i and nuclei I. Here $\hat{\zeta}(r_{iI})$ is an operator that is depends on the distance between electron i and nucleus I that is very strongly peaked at the origin ($r_{iI} = 0$). For the diagonal matrix elements of $\hat{H}^{SO}$, the only portion of the

$\hat{\boldsymbol{\ell}}_{iI} \cdot \hat{\mathbf{s}}_i$operator that contributes is the $\hat{\ell}_{iI,z}\hat{s}_{i,z}$ contribution, which is readily evaluated. The remaining components of $\hat{\boldsymbol{\ell}}_{iI} \cdot \hat{\mathbf{s}}_i$ couple a state defined by Λ to one with $\Lambda\pm1$, and are only important in off-diagonal matrix elements. Further, because the spin-orbit operator is well-approximated by this one-electron operator, the spin-orbit energy may be estimated as the sum of the individual one-electron contributions. Thus, the spin-orbit stabilization of the $^3\Delta_1$ level of WC may be written as

$$E^{(1)} = \langle 1\delta_{+2}\beta | \sum \hat{\zeta}(r_I)\hat{\ell}_{I,z}\hat{s}_z | 1\delta_{+2}\beta \rangle + \langle 3\sigma\beta | \sum \hat{\zeta}(r_I)\hat{\ell}_{I,z}\hat{s}_z | 3\sigma\beta \rangle, \quad (4.3)$$

where the unnecessary electron label, i, has been dropped and the summation is only over the nuclei, *I*. Recognizing that the spin-orbitals are eigenfunctions of $\hat{\ell}_{I,z}$ and $\hat{s}_z$, and absorbing the units of $\hbar$ into the definition of $\hat{\zeta}(r)$, this becomes

$$E^{(1)} = 2 \cdot \left(-\tfrac{1}{2}\right) \langle 1\delta_{+2} | \sum \hat{\zeta}(r_I) | 1\delta_{+2} \rangle + 0 \cdot \left(-\tfrac{1}{2}\right) \langle 3\sigma | \sum \hat{\zeta}(r_I) | 3\sigma \rangle, \quad (4.4)$$

or $$E^{(1)} = -\langle 1\delta_{+2} | \sum \hat{\zeta}(r_I) | 1\delta_{+2} \rangle = -\langle 1\delta_{+2} | \hat{\zeta}(r_W) | 1\delta_{+2} \rangle - \langle 1\delta_{+2} | \hat{\zeta}(r_C) | 1\delta_{+2} \rangle. \quad (4.5)$$

Here, the summation over nuclei has been explicitly written using the distance of the electron from the W and C nuclei, r_W and r_C, respectively. Further, because $\hat{\zeta}(r)$ is so strongly peaked at the nucleus, the orbitals may be decomposed into contributions from the corresponding atoms, in the spirit of the LCAO approximation, and contributions to the integrals involving functions localized on different atoms may be neglected. For the 1δ orbital, the contribution on carbon is negligible. Thus, we obtain

$$E^{(1)} = -\langle 5d\delta_{+2} | \hat{\zeta}(r_W) | 5d\delta_{+2} \rangle = -\zeta_{5d}(W). \quad (4.6)$$

In this result, the parameter $\zeta_{5d}(W)$ is a characteristic of the atomic 5*d* orbital of tungsten that may be obtained from atomic Hartree-Fock calculations or by fitting the

measured atomic energy levels.[25, 52, 53] If a partially occupied π orbital were present, it would be necessary to break $E^{(1)}$ down into contributions on W and C, as $|\pi\rangle = c_W|5d\pi\rangle + c_C|2p\pi\rangle$. In that event, the spin-orbit integral would retain contributions from both atoms, giving

$$\langle\pi|\sum \hat{\zeta}(r_I)|\pi\rangle = |c_W|^2\langle 5d\pi|\,\hat{\zeta}(r_W)|5d\pi\rangle + |c_C|^2\langle 2p\pi|\,\hat{\zeta}(r_C)|2p\pi\rangle$$
$$= |c_W|^2\,\zeta_{5d}(W) + |c_C|^2\zeta_{2p}(C)\,. \qquad (4.7)$$

3. Second-order corrections for Σ molecular states

For Σ terms that are candidates for the ground state, first-order perturbation theory predicts no spin-orbit splitting or stabilization. In these cases, one must go beyond first order. For the $1\sigma^2 1\pi^4 2\sigma^2 1\delta^2 3\sigma^2$, $^3\Sigma^-$ terms that are candidates for the WS and WSe ground states, an isoconfigurational spin-orbit interaction with the $1\sigma^2 1\pi^4 2\sigma^2 1\delta^2 3\sigma^2$, $^1\Sigma^+$ state leads to a significant stabilization of the $^3\Sigma^-$ ($\Omega=0^+$) component.[25] Using the methods described above, the spin-orbit interaction matrix element that couples the $^1\Sigma^+$ ($\Omega = 0^+$) state to the $^3\Sigma^-$ ($\Omega=0^+$) state, which is responsible for the stabilization of the $^3\Sigma^-$ ($\Omega=0^+$) state, may be readily derived as

$$\langle\, ^1\Sigma^+(0^+)|\hat{H}^{SO}|\, ^3\Sigma^-(0^+)\rangle = 2\zeta_{5d}(W). \qquad (4.8)$$

To evaluate the effect on the $^3\Sigma^-$ ($\Omega=0^+$) state, one must solve the two state matrix Hamiltonian problem

$$\underline{\underline{H}} = \begin{pmatrix} \Delta E & 2\zeta \\ 2\zeta & 0 \end{pmatrix} \quad , \qquad (4.9)$$

where ΔE represents the energy difference between the two coupled states, $\Delta E = E(^1\Sigma^+) - E(^3\Sigma^-)$. Because the energy of the $^3\Sigma^-$ state is defined as zero in this expression, the lower energy root,

$$E_{-} = \frac{1}{2}\left[\Delta E - \sqrt{(\Delta E)^2 + 16\zeta_W^2}\right], \tag{4.10}$$

provides the spin-orbit stabilization of the lower spin-orbit level ($\Omega=0^+$) of the $^3\Sigma^-$ term.

To complete the evaluation of the spin-orbit stabilization of the $^3\Sigma^-(0^+)$ level, we need the energy separation between the $^3\Sigma^-$ term and the $^1\Sigma^+$ term. Recognizing that these two terms differ by how the spins are coupled in a $1\delta_{+2}^{\ 1}\ 1\delta_{-2}^{\ 1}$ configuration, and that the 1δ orbital is very nearly a pure 5*d*δ orbital on W, we have used the numerical Hartree-Fock program HARTREE, written by Charlotte Froese-Fischer, to evaluate the expected splitting.[53] The result may be expressed in terms of the Slater $F^4(5d, 5d)$ radial integral as

$$\Delta E = \frac{20}{63}\, F^4(5d, 5d)\,, \tag{4.11}$$

where the factor of 20/63 results from angular integrals. Using an average of the $F^4(5d, 5d)$ integrals obtained from HARTREE for neutral and ionic (W and W^+) atoms, we obtain ΔE = 11,265 cm^{-1}. Using the average of the ζ_{5d}(W) values obtained for W and W^+ (ζ = 2259 cm^{-1}), a net spin-orbit stabilization of the $^3\Sigma^-(0^+)$ level of -1588 cm^{-1} (-0.197 eV) is obtained. This value is expected to be nearly the same for both WS and WSe because the 1δ orbital remains nearly purely tungsten 5*d*δ in both molecules. For comparison, a contracted multi-reference configuration interaction (CMRCI) on the congeneric WO molecule found that without spin-orbit interactions, the $^1\Sigma^+$ - $^3\Sigma^-$ separation is 7319 cm^{-1} (somewhat smaller than our value of 11,265 cm^{-1}).[45] When spin-orbit interactions are subsequently included, it was found that the $^3\Sigma^-(0^+)$ is stabilized more effectively, lying 1898 cm^{-1} below the $^3\Sigma^-(1)$ level.[45] For the $^3\Sigma^-(0^+)$ level of WO, the spin-orbit stabilization is thus calculated to be -0.235 eV. The simplified method described here, which gives -0.197 eV, is in tolerable agreement with this much more involved calculation.

Finally, we also consider the spin-orbit stabilization in the $1\sigma^2 1\pi^4 2\sigma^2 1\delta^2 3\sigma^1 2\pi^2$, $^6\Sigma^+$ ground state of WCl, which splits into Ω = 1/2, 3/2, and 5/2 levels when interactions with other states are considered. The $^6\Sigma^+$ state undergoes spin-orbit coupling to two $^4\Sigma^-$ states that derive from the same configuration, but whose energies are difficult to determine. For this reason, we have adopted a different method to approximate the spin-orbit stabilization of the expected $^6\Sigma^+(\Omega = ½)$ ground level. The spin-orbit splitting in the isovalent CrF and CrCl $^6\Sigma^+$ ground states has been measured, and is characterized by the molecular constant, λ. For a $^6\Sigma^+$ state, this term contributes to the Hamiltonian as $\frac{2}{3}\lambda\,(3\hat{S}_z^2 - \hat{S}^2)$, leading to a spin-orbit stabilization of the ground Ω = 1/2 level by of $-\frac{16}{3}\lambda$. For CrF and CrCl, the stabilization is -3.44 and -1.42 cm^{-1}, respectively. A portion of this stabilization derives from the direct interaction of the magnetic dipoles of the unpaired electrons, but this is generally smaller than the spin-orbit contribution for transition metal species. To estimate the spin-orbit stabilization of the ground $^6\Sigma^+(1/2)$ level in WCl, we have simply taken the stabilizations in CrF and CrCl, and scaled them by the ratio $[\zeta_{5d}(W)/\zeta_{3d}(Cr)]^2$. Given that the spin-orbit stabilization arises in second order perturbation theory, a dependence on ζ^2 is expected, so this approach is reasonable in the absence of more detailed calculations that are beyond the scope of this work. Using $\zeta_{3d}(Cr)$ = 233.5 cm^{-1} (average value for Cr and Cr^+) and $\zeta_{5d}(W)$ = 2259 cm^{-1} (average of values calculated for W and W^+), we obtain expected spin-orbit stabilizations for the $^6\Sigma^+(1/2)$ level of WCl of -322 cm^{-1} (scaled from CrF) or -133 cm^{-1} (scaled from CrCl). We adopt the average of these values, -228 cm^{-1} or -0.028 eV, as our best estimate of this correction.

Using these methods, spin-orbit corrections to calculated dissociation energies (D_0) are provided in Table 2. In all cases, these corrections worsen the agreement between the

computed values and experiment because the spin-orbit stabilization of the separated atoms is greater than that of the molecule. The reduction in bond dissociation energies due to spin-orbit effects has been discussed elsewhere,[54] and is generally expected in cases where the separated atoms states exhibit spin-orbit splitting. Overall, these results demonstrate that B3LYP/LANL2DZ computations are inadequate for the calculation of bond dissociation energies in diatomic tungsten compounds.

D. Derived Quantities

The measured BDEs may be combined with other values to obtain derived quantities, when the required other values are available. For the molecules investigated here, however, only a few related studies are available.

For WC, the BDE of the related molecule, WC^+ has been measured by guided ion beam mass spectrometry. An early investigation provided $D_0(W^+\text{-}C) = 5.01$ eV;[55] a subsequent study provided an improved value of 4.76(9) eV.[56] This value is somewhat less than the BDE of neutral WC obtained in this work, 5.289(8) eV, indicating that the bond weakens by 0.53(9) eV upon ionization. Using the thermochemical cycle,

$$D_0(WC) + IE(W) = IE(WC) + D_0(W^+\text{-}C), \qquad (4.12)$$

in combination with the ionization energy of W, IE(W) = 7.86403(10) eV,[57] this allows the determination of the ionization energy of WC as IE(WC) = 8.39(9) eV. This result is consistent with our previous observation of effective ionization of WC via a resonant two-photon ionization process employing a total 2-photon energy of 8.60 eV.[27]

A measurement of the electron affinity of WC, EA(WC) = 2.155(15) eV,[58] may also be combined with the electron affinity of carbon, EA(C) = 1.2629(3) eV,[59] using the thermochemical cycle

$$D_0(W\text{-}C^-) + EA(C) = EA(WC) + D_0(WC), \quad (4.13)$$

to deduce the BDE of WC^- as $D_0(W\text{-}C^-) = 6.181(17)$ eV. Using EA(W) = 0.815(8) eV,[59] a similar thermochemical cycle provides $D_0(W^-\text{-}C) = 7.363(19)$ eV. As is the case for many anions, a much lower energy decomposition pathway for the anion is loss of an electron, rather than dissociation.

In the case of WSi, a previous study of the WSi^- anion has provided the vertical detachment energy of 1.72(4) eV.[33] This result provides a constraint on the adiabatic electron affinity of EA(WSi) ≤ 1.72(4) eV. Again, using a thermochemical cycle analogous to (4.13), in combination with the electron affinity of Si, EA(Si) = 1.385(5) eV,[59] the BDE of the WSi^- anion is obtained as $D_0(W\text{-}Si^-) \leq 3.44(4)$ eV. Using EA(W) = 0.815(8) eV,[59] a similar thermochemical cycle provides $D_0(W^-\text{-}Si) \leq 4.01(4)$ eV.

Finally, the 0K enthalpies of formation of these WX molecules may be calculated from the atomic enthalpies of formation using

$$\Delta_f H^\circ_{0K}(WX) = \Delta_f H^\circ_{0K}(W) + \Delta_f H^\circ_{0K}(X) - D_0(WX). \quad (4.14)$$

Atomic enthapies of formation have been taken from the NIST JANAF tables (Ref. 60) and in the case of Se, from a Russian compilation.[61] The results are provided in Table 3.

V. DISCUSSION

To our knowledge, this article provides the first measurement of the bond energies of the WC, WSi, WS, WSe, and WCl molecules. Our previous reports on the BDEs of the group 4 and 5 silicides and selenides,[2, 4] along with an upcoming report on the BDEs of the group 4 and group 5 carbides (unpublished) allow these new results to be placed in context. The trends among the HfX, TaX, WX molecules are displayed in Table 4.

A striking trend among the HfX, TaX, WX molecules is that the BDEs of the carbides, and to a lesser extent the silicides, increase in moving from Hf to Ta to W, while the BDEs of the selenides decrease uniformly across the series. The trend of increasing BDE as one moves from the left to the right in the transition metal series is also observed for the 5d cations, MC^+,[62] for the neutral 4d MC molecules,[63], and for the 4d and 5d MSi and MSi^+ species (with exceptions for atoms with nd^5 configurations).[32] Conversely, the trend of decreasing BDE as one moves from the left to the right is also observed for the 3d MO, MO^+, MS, and MS^+ molecules,[64-66] as well as for the 4d MO^+ and MS^+ species.[66]

While the chemical bonding in these molecules is quite complicated,[65] the bonding trends between M^+ ions and s^2p^2 elements like C and Si have been rationalized in a valence bond framework through the observation that these ligands can form two bonds to the metal by spin-pairing the unpaired *p* electrons with unpaired metal *d* electrons, but a third bond can be fully formed only if a doubly-occupied *d* orbital is present on the metal to donate into the empty *p* orbital of the ligand.[62] Thus, the most strongly bound MC and MSi species are those with at least one doubly-occupied *d* orbital, i.e., those with d^6 through d^8 configurations.[62] The resulting bonds are particularly strong for transition metals with larger, more accessible *d* orbitals, the 4*d* and 5*d* metals. In cases where there are insufficient *d* electrons, as in ScC for example,[67] the doubly-occupied 4*s* orbital can substitute for a doubly-occupied *d*σ orbital; the poor orbital overlap results in a weak bond, however. In other cases, such as TiC,[68] where the ground state is formed by the interaction of a $3d^34s^1$, ^{3}F atom with carbon, the bond is weakened by the promotion energy required to prepare the metal atom for bonding.

In the transition metal chalcogenides, MO, MS, and MSe, the ligand atom has an ns^2np^4 ground configuration, and bonding occurs by spin-pairing two unpaired n*p* electrons

with two unpaired *d* electrons, and donating the remaining pair of n*p* electrons into an empty *d* orbital, resulting in a triple bond.[64, 69] Such an arrangement requires at least two unpaired *d* electrons and one empty *d* orbital, implying that configurations of d^2 through d^4 are optimal. Late transition metals with configurations with 5 or more *d* electrons are incapable of forming a triple bond, leading to a reduction in the BDE. While these ideas explain the broad trend in bond dissociation energies across the transition metal series, the details vary substantially from molecule to molecule, in part because the ground state of the molecule may derive from a promoted state of the transition metal atom.

VI. CONCLUSION

Predissociation thresholds have been found in the resonant two-photon ionization spectra of WC, WSi, WS, WSe, and WCl. At a minimum, these provide upper limits on the bond dissociation energies of these molecules. Based on the density of vibronic levels and the degree of spectral congestion, however, we believe that the observed predissociation thresholds correspond closely to the thermochemical bond dissociation energies (BDEs) of these species. The measured BDEs have been combined with related information to provide values of IE(WC), $D_0(W\text{-}C^-)$, $D_0(W^-\text{-}C)$, $D_0(W\text{-}Si^-)$, and $D_0(W^-\text{-}Si)$, along with 0K enthalpies of formation of all five gaseous molecules.

AUTHOR INFORMATION

Corresponding Author

*E-mail: morse@chem.utah.edu . Fax: (801)-581-8433

Notes:

The authors declare no competing financial interest.

ACKNOWLEDGMENT

The authors thank the National Science Foundation for support of this research under Grant No. CHE-1664962.

REFERENCES

(1) Johnson, E. L.; Davis, Q. C.; Morse, M. D. Predissociation measurements of bond dissociation energies: VC, VN, and VS. *J. Chem. Phys.* **2016**, *144*, 234306.

(2) Sorensen, J. J.; Persinger, T. D.; Sevy, A.; Franchina, J. A.; Johnson, E. L.; Morse, M. D. Bond dissociation energies of diatomic transition metal selenides: TiSe, ZrSe, HfSe, VSe, NbSe, and TaSe. *J. Chem. Phys.* **2016**, *145*, 214308.

(3) Matthew, D. J.; Tieu, E.; Morse, M. D. Determination of the bond dissociation energies of FeX and NiX (X = C, S, Se). *J. Chem. Phys.* **2017**, *146*, 144310.

(4) Sevy, A.; Sorensen, J. J.; Persinger, T. D.; Franchina, J. A.; Johnson, E. L.; Morse, M. D. Bond dissociation energies of diatomic transition metal silicides: TiSi, ZrSi, HfSi, VSi, NbSi, and TaSi. *J. Chem. Phys.* **2017**, *147*, 084301.

(5) Taylor, S.; Spain, E. M.; Morse, M. D. Resonant two-photon ionization spectroscopy of jet-cooled NiPt. *J. Chem. Phys.* **1990**, *92*, 2698-2709.

(6) Behm, J. M.; Arrington, C. A.; Morse, M. D. Spectroscopic studies of jet-cooled AlNi. *J. Chem. Phys.* **1993**, *99*, 6409-6415.

(7) Russon, L. M.; Heidecke, S. A.; Birke, M. K.; Conceicao, J.; Armentrout, P. B.; Morse, M. D. The bond strength of Co_2^+. *Chem. Phys. Lett.* **1993**, *204*, 235-240.

(8) Spain, E. M.; Morse, M. D. Bond strengths of transition metal diatomics: VNi and V_2. *Int. J. Mass. Spectrom. Ion Proc.* **1990**, *102*, 183-197.

(9) Spain, E. M.; Morse, M. D. Bond strengths of transition metal dimers: TiV, V_2, TiCo, and VNi. *J. Phys. Chem.* **1992**, *96*, 2479-2486.

(10) Arrington, C. A.; Blume, T.; Morse, M. D.; Doverstål, M.; Sassenberg, U. Bond strengths of transition metal diatomics: Zr_2, YCo, YNi, ZrCo, ZrNi, NbCo, and NbNi. *J. Phys. Chem.* **1994**, *98*, 1398-1406.

(11) Fu, Z.; Russon, L. M.; Morse, M. D.; Armentrout, P. B. Photodissociation measurements of bond dissociation energies: $D_0(Al_2\text{-}Al)$, $D_0(TiO^+\text{-}Mn)$, and $D_0(V_2^+\text{-}V)$. *Int. J. Mass Spectrom.* **2001**, *204*, 143-157.

(12) Russon, L. M.; Heidecke, S. A.; Birke, M. K.; Conceicao, J.; Morse, M. D.; Armentrout, P. B. Photodissociation measurements of bond dissociation energies: Ti_2^+, V_2^+, Co_2^+, and Co_3^+. *J. Chem. Phys.* **1994**, *100*, 4747-4755.

(13) James, A. M.; Kowalczyk, P.; Langlois, E.; Campbell, M. D.; Ogawa, A.; Simard, B. Resonant two photon ionization spectroscopy of the molecules V_2, VNb, Nb_2. *J. Chem. Phys.* **1994**, *101*, 4485-4495.

(14) Yang, D. S.; James, A. M.; Rayner, D. M.; Hackett, P. A. Pulsed field ionization zero kinetic energy photoelectron spectroscopy of the vanadium dimer molecule. *J. Chem. Phys.* **1995**, *102*, 3129-3134.

(15) Manivasagam, S.; Laury, M. L.; Wilson, A. K. Pseudopotential-Based Correlation Consistent Composite Approach (rp-ccCA) for First- and Second-Row Transition Metal Thermochemistry. *J. Phys. Chem. A* **2015**, *119*, 6867-6874.

(16) Xu, X.; Zhang, W.; Tang, M.; Truhlar, D. G. Do Practical Standard Coupled Cluster Calculations Agree Better than Kohn-Sham Calculations with Currently Available Functionals When Compared to the Best Available Experimental Data for Dissociation Energies of Bonds to 3d Transition Metals? *J. Chem. Theory Comput.* **2015**, *11*, 2036-2052.

(17) Laury, M. L.; Wilson, A. K. Performance of Density Functional Theory for Second Row (4d) Transition Metal Thermochemistry. *J. Chem. Theory Comput.* **2013**, *9*, 3939-3946.

(18) Wiley, W. C.; McLaren, I. H. Time-of-Flight Mass Spectrometer with Improved Resolution. *Rev. Sci. Instrum.* **1955**, *26*, 1150 - 1157.

(19) Mamyrin, B. A.; Karataev, V. I.; Shmikk, D. V.; Zagulin, V. A. Mass reflectron. New nonmagnetic time-of-flight high-resolution mass spectrometer. *Zh. Eksp. Teor. Fiz.* **1973**, *64*, 82-89.

(20) Kramida, A.; Ralchenko, Y.; Reader, J.; and NIST ASD Team, *Atomic Spectra Database (version 5.5.1)*; National Institute of Standards and Technology, Gaithersburg, MD, 2017. https://physics.nist.gov/asd

(21) Frisch, M. J.; Trucks, G. W.; Schlegel, H. B.; Scuseria, G. E.; Robb, M. A.; Cheeseman, J. R.; Scalmani, G.; Barone, V.; Mennucci, B.; Petersson, G. A.; *et al.* Gaussian 09, Revision D.01; Gaussian, Inc.: Wallingford, CT, 2009.

(22) Hay, P. J.; Wadt, W. R. Ab initio effective core potentials for molecular calculations. Potentials for potassium to gold including the outermost core orbitals. *J. Chem. Phys.* **1985**, *82*, 299-310.

(23) Lee, C.; Yang, W.; Parr, R. G. Development of the Colle-Salvetti correlation-energy formula into a functional of the electron density. *Phys. Rev. B: Condens. Matter* **1988**, *37*, 785-789.

(24) Becke, A. D. Density-functional thermochemistry. III. The role of exact exchange. *J. Chem. Phys.* **1993**, *98*, 5648-5652.

(25) Lefebvre-Brion, H.; Field, R. W. *The Spectra and Dynamics of Diatomic Molecules*; Elsevier: Amsterdam, 2004.

(26) Herzberg, G. *Molecular Spectra and Molecular Structure I. Spectra of Diatomic Molecules*, 2nd ed.; Van Nostrand Reinhold: New York, 1950.

(27) Sickafoose, S. M.; Smith, A. W.; Morse, M. D. Optical spectroscopy of tungsten carbide (WC). *J. Chem. Phys.* **2002**, *116*, 993-1002.

(28) Wang, F.; Steimle, T. C. Optical Zeeman spectroscopy of the [17.6]2-$X^3\Delta_1$(1,0) band system of tungsten monocarbide, WC. *J. Chem. Phys.* **2011**, *135*, 104313.

(29) Wang, F.; Steimle, T. C. Communication: Electric dipole moment and hyperfine interaction of tungsten monocarbide, WC. *J. Chem. Phys.* **2011**, *134*, 201106.

(30) Wang, F.; Steimle, T. C. Tungsten monocarbide, WC: Pure rotational spectrum and ^{13}C hyperfine interaction. *J. Chem. Phys.* **2012**, *136*, 044312.

(31) Yuan, Z. S.; Zhu, L. F.; Tong, X.; Li, W. B.; Liu, X. J.; Xu, K. Z. Which is the most stable one in WSi_n (n=1-4)? A density functional investigation with pseudo-potential model. *J. Mol. Struct. THEOCHEM* **2002**, *589-590*, 229-237.

(32) Wu, Z. J.; Su, Z. M. Electronic structures and chemical bonding in transition metal monosilicides MSi (M=3d, 4d, 5d elements). *J. Chem. Phys.* **2006**, *124*, 184306.

(33) Gunaratne, K. D. D.; Berkdemir, C.; Harmon, C. L.; Castleman, A. W. Probing the valence orbitals of transition metal-silicon diatomic anions. ZrSi, NbSi, MoSi, PdSi and WSi. *Phys. Chem. Chem. Phys.* **2013**, *15*, 6068-6079.

(34) Lee, J.; Meyer, E. R.; Paudel, R.; Bohn, J. L.; Leanhardt, A. E. An electron electric dipole moment search in the $X^3\Delta_1$ ground state of tungsten carbide molecules. *J. Mod. Opt.* **2009**, *56*, 2005-2012.

(35) Lee, J.; Chen, J.; Skripnikov, L. V.; Petrov, A. N.; Titov, A. V.; Mosyagin, N. S.; Leanhardt, A. E. Optical Spectroscopy of Tungsten Carbide for Uncertainty Analysis in Electron Electric-Dipole-Moment Search. *Phys. Rev. A At., Mol., Opt. Phys.* **2013**, *87*, 022516.

(36) Wang, J.; Sun, X.; Wu, Z. Theoretical Investigation of 5d-Metal Monocarbides. *J. Cluster Sci.* **2007**, *18*, 333-344.

(37) Balasubramanian, K. Spectroscopic Constants and Potential Energy Curves of Tungsten Carbide. *J. Chem. Phys.* **2000**, *112*, 7425-7436.

(38) Hocking, W. H.; Merer, A. J.; Milton, D. J.; Jones, W. E.; Krishnamurty, G. Laser-Induced Fluorescence and Discharge Emission Spectra of CrO. Rotational Analysis of the A $^5\Pi$-X $^5\Pi$ Transition. *Can. J. Phys.* **1980**, *58*, 516-533.

(39) Shi, Q.; Ran, Q.; Tam, W. S.; Leung, J. W. H.; Cheung, A. S. C. Laser-Induced Fluorescence Spectroscopy of CrS. *Chem. Phys. Lett.* **2001**, *339*, 154-160.

(40) Pulliam, R. L.; Ziurys, L. M. The Pure Rotational Spectrum of the CrS Radical in its X $^5\Pi_r$ state. *J. Chem. Phys.* **2010**, *133*, 174313.

(41) Hamrick, Y. M.; Taylor, S.; Morse, M. D. Optical Spectroscopy of Jet-Cooled MoO. *J. Mol. Spectrosc.* **1991**, *146*, 274-313.

(42) Langhoff, S. R.; Bauschlicher, C. W., Jr.; Pettersson, L. G. M.; Siegbahn, P. E. M. Theoretical Spectroscopic Constants for the Low-Lying States of the Oxides and Sulfides of Mo and Tc. *Chem. Phys.* **1989**, *132*, 49-58.

(43) Sun, X.; Wang, J.; Wu, Z. Chemical Bonding and Electronic Structure of 4d-Metal Monosulfides. *J. Cluster Sci.* **2009**, *20*, 525-534.

(44) Ram, R. S.; Lievin, J.; Li, G.; Hirao, T.; Bernath, P. F. The $X^3\Sigma^-$ Ground State of WO. *Chem. Phys. Lett.* **2001**, *343*, 437-445.

(45) Ram, R. S.; Lievin, J.; Bernath, P. F. Fourier Transform Emission Spectroscopy and Ab Initio Calculations on WO. *J. Mol. Spectrosc.* **2009**, *256*, 216-227.

(46) Launila, O. Spectroscopy of CrF: Rotational Analysis of the $A^6\Sigma^+$ - $X^6\Sigma^+$ Band System in the 1 μm Region. *J. Mol. Spectrosc.* **1995**, *169*, 373-395.

(47) Okabayashi, T.; Tanimoto, M. The Rotational Spectrum of the CrF Radical in the X $^6\Sigma^+$ state. *J. Chem. Phys.* **1996**, *105*, 7421-7424.

(48) Bencheikh, M.; Koivisto, R.; Launila, O.; Flament, J. P. The Low-Lying Electronic States of CrF and CrCl: Analysis of the $A^6\Sigma^+$ -- $X^6\Sigma^+$ System of CrCl. *J. Chem. Phys.* **1997**, *106*, 6231-6239.

(49) Oike, T.; Okabayashi, T.; Tanimoto, M. Millimeter-Wave Spectroscopy of Chromium Monochloride (CrCl). *J. Chem. Phys.* **1998**, *109*, 3501-3507.

(50) Cheng, L.; Wang, M. Y.; Wu, Z. J.; Su, Z. M. Electronic Structures and Chemical Bonding in 4d Transition Metal Monohalides. *J. Comput. Chem.* **2007**, *28*, 2190-2202.

(51) Kalamse, V.; Wadnerkar, N.; Chaudhari, A. Theoretical Study of Third-Row Transition Metal Monofluorides. *Int. J. Quantum Chem.* **2011**, *111*, 2014-2020.

(52) Fischer, C. F. Average-Energy-of-Configuration. Hartree-Fock Results for the Atoms Helium to Radon. *At. Data* **1972**, *4*, 301-399.

(53) Fischer, C. F. *The Hartree-Fock Method for Atoms*; John Wiley & Sons: New York, 1977.

(54) Balasubramanian, K. Relativity and Chemical Bonding. *J. Phys. Chem.* **1989**, *93*, 6585-6596.

(55) Armentrout, P. B.; Zhang, X. G.; Shin, S. Inorganic Mass Spectrometry: Reactions of Third-Row Transition-Metal Ions with Methane. *Adv. Mass Spectrom.* **2001**, *15*, 89-99.

(56) Hinton, C. S.; Li, F.; Armentrout, P. B. Reactions of Hf^+, Ta^+, and W^+ with O_2 and CO: Metal Carbide and Metal Oxide Cation Bond Energies. *Int. J. Mass Spectrom.* **2009**, *280*, 226-234.

(57) Campbell-Miller, M. D.; Simard, B. First Ionization Potentials of Tungsten and Rhenium by Mass-Selected Double-Resonance Ionization Spectroscopy. *J. Opt. Soc. Am. B: Opt. Phys.* **1996**, *13*, 2115-2120.

(58) Rothgeb, D.; Hossain, E.; Jarrold, C. C. Tungsten Carbide Revisited: New Anion Photoelectron Spectrum and Density Functional Theory Calculations. *J. Chem. Phys.* **2008**, *129*, 114304.

(59) Hotop, H.; Lineberger, W. C. Binding Energies in Atomic Negative Ions: II. *J. Phys. Chem. Ref. Data* **1985**, *14*, 731-750.

(60) Chase, M. W., Jr. *NIST-JANAF Thermochemical Tables, Fourth Edition*; American Institute of Physics for the National Institute of Standards and Technology: Washington, D.C., 1998.

(61) Gurvich, L. V.; Karachevtsev, G. V.; Kondratyev, V. N.; Lebedev, Y.; Medvedev, V. A.; Potapov, V.; Hodeev, S. *Bond Energies of Chemical Bonds, Ionization Potentials and Electron Affinities*; Nauka: Moscow, 1974.

(62) Armentrout, P. B. Methane Activation by 5d Transition Metals: Energetics, Mechanisms, and Periodic Trends. *Chem. - Eur. J.* **2017**, *23*, 10-18.

(63) Wang, J.; Sun, X.; Wu, Z. Chemical Bonding and Electronic Structure of 4d-Metal Monocarbides. *Chem. Phys. Lett.* **2006**, *426*, 141-147.

(64) Kretzschmar, I.; Schroder, D.; Schwarz, H.; Armentrout, P. B. The Binding in Neutral and Cationic 3d and 4d Transition-Metal Monoxides and -Sulfides. *Adv. Met. Semicond. Clusters* **2001**, *5*(Metal Ion Solvation and Metal-Ligand Interactions), 347-395.

(65) Gutsev, G. L.; Andrews, L.; Bauschlicher, C. W., Jr. Similarities and Differences in the Structure of 3d-Metal Monocarbides and Monoxides. *Theor. Chem. Acc.* **2003**, *109*, 298-308.

(66) Armentrout, P. B. Guided Ion Beam Studies of Transition Metal-Ligand Thermochemistry. *Int. J. Mass Spectrom.* **2003**, *227*, 289-302.

(67) Kalemos, A.; Mavridis, A.; Harrison, J. F. Theoretical Investigation of Scandium Carbide, ScC. *J. Phys. Chem. A* **2001**, *105*, 755-759.

(68) Kalemos, A.; Mavridis, A. Theoretical Investigation of Titanium Carbide, TiC: $X^3\Sigma^+$, $a^1\Sigma^+$, $A^3\Delta$, and $b^1\Delta$ States. *J. Phys. Chem. A* **2002**, *106*, 3905-3908.

(69) Carter, E. A.; Goddard, W. A., III. Early- Versus Late-Transition-Metal-Oxo Bonds: the Electronic Structure of VO^+ and RuO^+. *J. Phys. Chem.* **1988**, *92*, 2109-2115.

Table 1. Calculated electronic states of the WX molecules.

Molecule D_0(exp) [a]	Configuration[b]	Term	Energy (T_0, eV)	Dipole Moment (Debye)	ω_e [c] (cm^{-1})	r_e [c] (Å)	D_0 [c] (eV)	<S> [d]
WC	$1\sigma^2 1\pi^4 2\sigma^2 1\delta^1 3\sigma^1$	$^3\Delta$	0.00	4.23	987.1	1.736	4.90	1.010
5.289(8)	$1\sigma^2 1\pi^4 2\sigma^2 1\delta^2$	$^3\Sigma^-$	0.26	4.02	934.8	1.762	4.65	1.326
	$1\sigma^2 1\pi^4 2\sigma^1 1\delta^2 3\sigma^1$	$^5\Sigma^-$	0.26	3.28	1029.3	1.770	4.64	2.008
	$1\sigma^2 1\pi^4 2\sigma^2 3\sigma^2$	$^1\Sigma^+$	0.68	3.07	1076.4	1.753	4.22	0.000
	$1\sigma^2 1\pi^3 2\sigma^2 1\delta^1 3\sigma^2$	$^3\Pi/^3\Phi$	1.10	2.82	943.7	1.846	3.81	1.006
	$1\sigma^2 1\pi^4 2\sigma^1 1\delta^1 3\sigma^1 2\pi^1$	$^5\Pi/^5\Phi$	2.35	2.48	955.4	1.803	2.55	2.002
	$1\sigma^2 1\pi^4 2\sigma^2 1\delta^1 2\pi^1$	$^3\Pi/^3\Phi$	2.52	2.94	938.0	1.766	2.38	1.281
WSi	$1\sigma^2 1\pi^4 2\sigma^2 1\delta^1 3\sigma^1$	$^3\Delta$	0.00	2.43	456.9	2.245	2.77	1.043
3.103(10)	$1\sigma^2 1\pi^4 2\sigma^1 1\delta^2 3\sigma^1$	$^5\Sigma^-$	0.38	2.22	418.5	2.239	2.39	2.072
	$1\sigma^2 1\pi^3 2\sigma^2 1\delta^1 3\sigma^2$	$^3\Pi/^3\Phi$	0.58	1.58	428.0	2.307	2.19	1.026
	$1\sigma^2 1\pi^4 2\sigma^1 1\delta^1 3\sigma^1 2\pi^1$	$^5\Pi/^5\Phi$	2.05	1.77	451.5	2.243	0.72	2.009
	$1\sigma^2 1\pi^4 2\sigma^2 1\delta^1 2\pi^1$	$^3\Pi/^3\Phi$	2.29	1.51	354.9	2.301	0.48	1.260
WS	$1\sigma^2 1\pi^4 2\sigma^2 1\delta^2 3\sigma^2$	$^3\Sigma^-$	0.00	2.60	552.6	2.118	4.10	1.031
4.935(3)	$1\sigma^2 1\pi^4 2\sigma^2 1\delta^2 3\sigma^1 2\pi^1$	$^5\Pi$	0.09	4.18	476.4	2.192	4.02	2.018
	$1\sigma^2 1\pi^4 2\sigma^2 1\delta^2 3\sigma^2$	$^1\Sigma^+/^1\Gamma$	0.83	2.76	570.1	2.110	3.28	0.000
	$1\sigma^2 1\pi^4 2\sigma^2 1\delta^3 3\sigma^1$	$^3\Delta$	1.19	3.89	541.6	2.134	2.91	1.009
	$1\sigma^2 1\pi^4 2\sigma^2 1\delta^1 3\sigma^1 2\pi^2$	$^5\Delta$	1.32	4.47	462.9	2.231	2.79	2.003
	$1\sigma^2 1\pi^4 2\sigma^2 1\delta^2 3\sigma^1 2\pi^1$	$^3\Pi/^3\Phi/^3H$	1.68	3.98	501.6	2.178	2.42	1.005
WSe	$1\sigma^2 1\pi^4 2\sigma^2 1\delta^2 3\sigma^1 2\pi^1$	$^5\Pi$	0.00	3.86	300.3	2.318	3.59	2.026
4.333(6)	$1\sigma^2 1\pi^4 2\sigma^2 1\delta^2 3\sigma^2$	$^3\Sigma^-$	0.05	2.18	350.1	2.241	3.55	1.042
	$1\sigma^2 1\pi^4 2\sigma^2 1\delta^2 3\sigma^2$	$^1\Sigma^+/^1\Gamma$	0.88	2.38	366.0	2.229	2.72	0.000
	$1\sigma^2 1\pi^4 2\sigma^2 1\delta^1 3\sigma^1 2\pi^2$	$^5\Delta$	1.16	4.21	300.3	2.350	2.44	2.003
	$1\sigma^2 1\pi^4 2\sigma^2 1\delta^3 3\sigma^1$	$^3\Delta$	1.23	3.49	345.5	2.257	2.37	1.013
	$1\sigma^2 1\pi^4 2\sigma^2 1\delta^2 3\sigma^1 2\pi^1$	$^3\Pi/^3\Phi/^3H$	1.61	3.66	321.9	2.300	1.98	1.007
WCl	$1\sigma^2 1\pi^4 2\sigma^2 1\delta^2 3\sigma^1 2\pi^2$	$^6\Sigma^+$	0.00	3.91	348.2	2.360	3.80	2.501
3.818(6)	$1\sigma^2 1\pi^4 2\sigma^2 1\delta^1 3\sigma^2 2\pi^2$	$^4\Delta$	0.84	3.13	368.7	2.322	2.96	1.502
	$1\sigma^2 1\pi^4 2\sigma^2 1\delta^2 3\sigma^1 2\pi^1 4\sigma^1$	$^6\Pi$	1.04	2.33	295.8	2.449	2.76	2.503
	$1\sigma^2 1\pi^4 2\sigma^2 1\delta^2 3\sigma^2 2\pi^1$	$^2\Pi/^2\Phi/^2H$	1.43	2.56	396.5	2.263	2.37	0.915
	$1\sigma^2 1\pi^4 2\sigma^2 1\delta^2 3\sigma^2 2\pi^1$	$^2\Pi$	1.50	2.09	376.0	2.274	2.30	0.974
	$1\sigma^2 1\pi^4 2\sigma^2 1\delta^1 3\sigma^1 2\pi^2 4\sigma^1$	$^6\Delta$	1.68	3.07	281.5	2.510	2.12	2.500
	$1\sigma^2 1\pi^4 2\sigma^2 1\delta^2 3\sigma^2 2\pi^1$	$^4\Pi$	1.79	2.28	302.3	2.401	2.01	1.701
	$1\sigma^2 1\pi^4 2\sigma^2 1\delta^2 3\sigma^1 2\pi^2$	$^4\Sigma^-/^4\Gamma$	1.85	3.56	350.4	2.354	1.95	1.501

[a] For comparison, the bond dissociation energy measured in the present study is listed below the molecule for each species, in units of eV.

[b] Orbitals are listed in a uniform order within a configuration for comparison purposes.

[c] The computed quantities ω_e, r_e, and D_0 refer to the harmonic vibrational frequency, the equilibrium bond length, and the energy difference between the v=0 vibrational level and the ground separated atom limit, omitting spin-orbit effects, respectively.

[d] Calculations were done using the unrestricted B3LYP method, and expectation values of $\hat{\mathbf{S}}^2$ were equated to S(S+1) and solved for S. This is listed here as <S>. Values that differ significantly from the expected values of S = 0, 1, 2 (for WC, WSi, WS, or WSe) or S = 0.5, 1.5, 2.5 (for WCl) are indicative of problems with the computational method.

Table 2. Estimated spin-orbit corrections to calculated bond dissociation energies (eV) [a]

Molecule D_0(exp)	Configuration	Level	ΔE_{SO} (molecule) formula	ΔE_{SO} (molecule)	ΔE_{SO} (atoms)	Net ΔD_0	Uncorrected/Corrected D_0(computed)
WC	$1\delta^1\ 3\sigma^1$	$^3\Delta_1$	$-\zeta_W$	-0.280	-0.556	-0.276	4.90/4.62
5.289(8)	$1\delta^2$	$^3\Sigma^-$ (0^+)	See text, Eqn (4.10)	-0.197	-0.556	-0.359	4.65/4.29
WSi	$1\delta^1\ 3\sigma^1$	$^3\Delta_1$	$-\zeta_W$	-0.280	-0.568	-0.288	2.77/2.48
3.103(10)							
WS	$1\delta^2$	$^3\Sigma^-(0^+)$	See text, Eqn (4.10)	-0.197	-0.572	-0.375	4.10/3.73
4.935(3)	$1\delta^2\ 3\sigma^1 2\pi^1$	$^5\Pi_{-1}$	$-[\lvert c_W\rvert^2\zeta_W + \lvert c_S\rvert^2\zeta_S]/2$	-0.186	-0.572	-0.386	4.02/3.63
WSe	$1\delta^2\ 3\sigma^1 2\pi^1$	$^5\Pi_{-1}$	$-[\lvert c_W\rvert^2\zeta_W + \lvert c_{Se}\rvert^2\zeta_{Se}]/2$	-0.248	-0.648	-0.400	3.59/3.19
4.333(6)	$1\delta^2$	$^3\Sigma^-(0^+)$	See text, Eqn (4.10)	-0.197	-0.648	-0.451	3.55/3.10
WCl	$1\delta^2\ 3\sigma^1\ 2\pi^2$	$^6\Sigma^+_{1/2}$	See text	-0.028	-0.577	-0.549	3.80/3.25
3.818(6)							

[a] Molecular spin-orbit stabilization energies (ΔE_{SO}(molecule)) were calculated using: $\zeta_W(5d)$ = 2259 cm^{-1} (abbreviated as ζ_W above, taken as the mean of the two values reported in reference 25); $\zeta_S(3p)$ = 354 cm^{-1} (abbreviated as ζ_S, taken as the mean of the values reported for S and S$^-$ in reference 25); and $\zeta_{Se}(3p)$ = 1604 cm^{-1} (abbreviated as ζ_{Se}, taken as the mean of the values reported for Se and Se$^-$ in reference 25). For the $^5\Pi$ terms of WS and WSe, the coefficients were estimated on the basis of B3LYP/LANL2DZ calculations as $|c_W|^2 = 0.6$ and and $\left|c_{S/Se}\right|^2 = 0.4$ for both WS and WSe, since negligible differences were found between the two species.

Table 3. Enthalpies of formation at 0K of gaseous WC, WSi, WS, WSe, and WCl.

$\Delta_f H^\circ_{0K}$ (kJ mol^{-1})		C	Si	S	Se	Cl
		711.185(0.46)	**445.668(8.0)**	**274.735(0.25)**	**235.4(1.5)**	**119.621(0.006)**
W	**849.782(6.3)**	1050.7(6.4)	996.1(10.2)	648.4(6.3)	667.1(6.5)	601.0(6.3)

[a] The values along the perimeter, in **bold**, are the atomic enthalpies of formation used in the calculations, taken from References 60 and 61.

Table 4. Bond dissociation energies of HfX, TaX, and WX.

D_0(MX) (eV)	Hf	Ta	W
C	4.426(3)[a]	4.975(3)[a]	5.289(8)[a]
Si	2.871(3)[b]	2.999(3)[b]	3.103(10)[b]
Se	5.154(4)[c]	4.705(3)[c]	4.333(6)[c]

[a] unpublished.

[a] From Reference 4.

[a] From Reference 2.

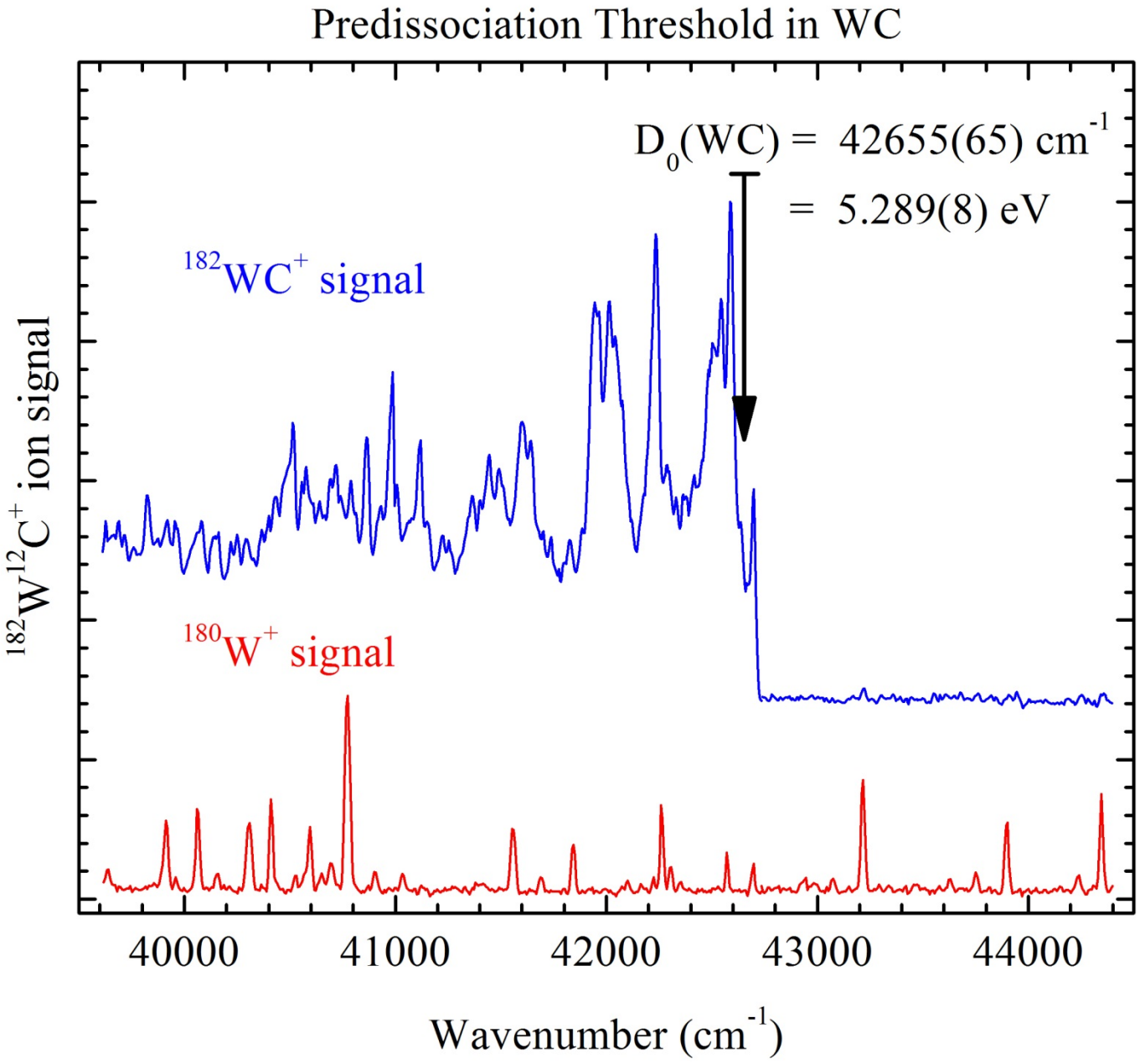

Figure 1. R2PI spectrum of tungsten carbide (WC), showing the predissociation threshold at 42,655 (65) cm^{-1}. The uncertainty range (±65 cm^{-1}) is indicated by the horizontal bar above the arrow showing the location of the predissociation threshold. Calibration of the spectrum was achieved using the ^{180}W lines, with confirmation from spectra recorded for ^{58}Ni.

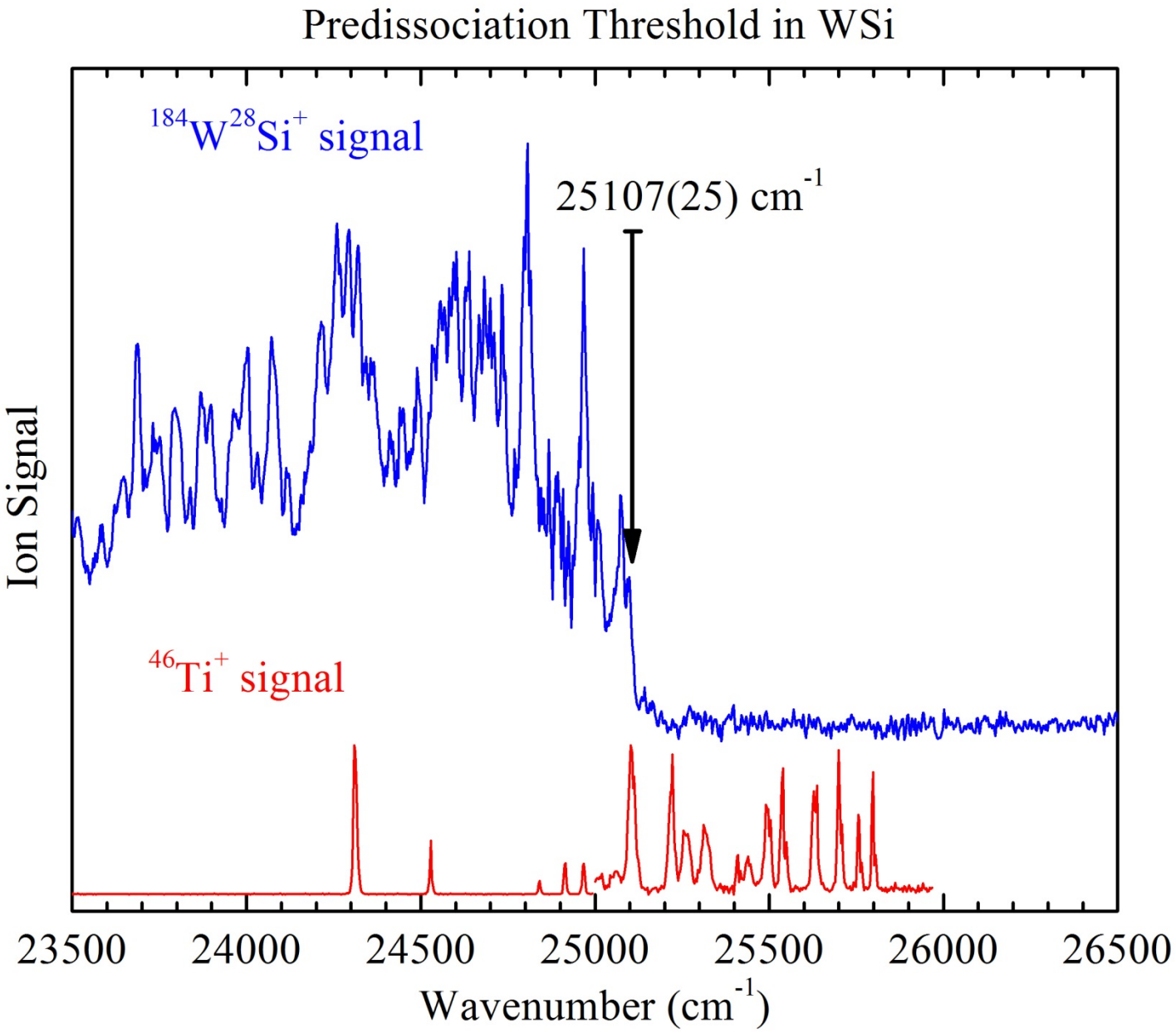

Figure 2. R2PI spectrum of tungsten silicide (WSi), showing the predissociation threshold at 25,107(25) cm^{-1}. The uncertainty range (±25 cm^{-1}) is indicated by the horizontal bar above the arrow showing the location of the predissociation threshold. A scan using a Ti sample was used to obtain atomic transitions for calibration in this spectral range.

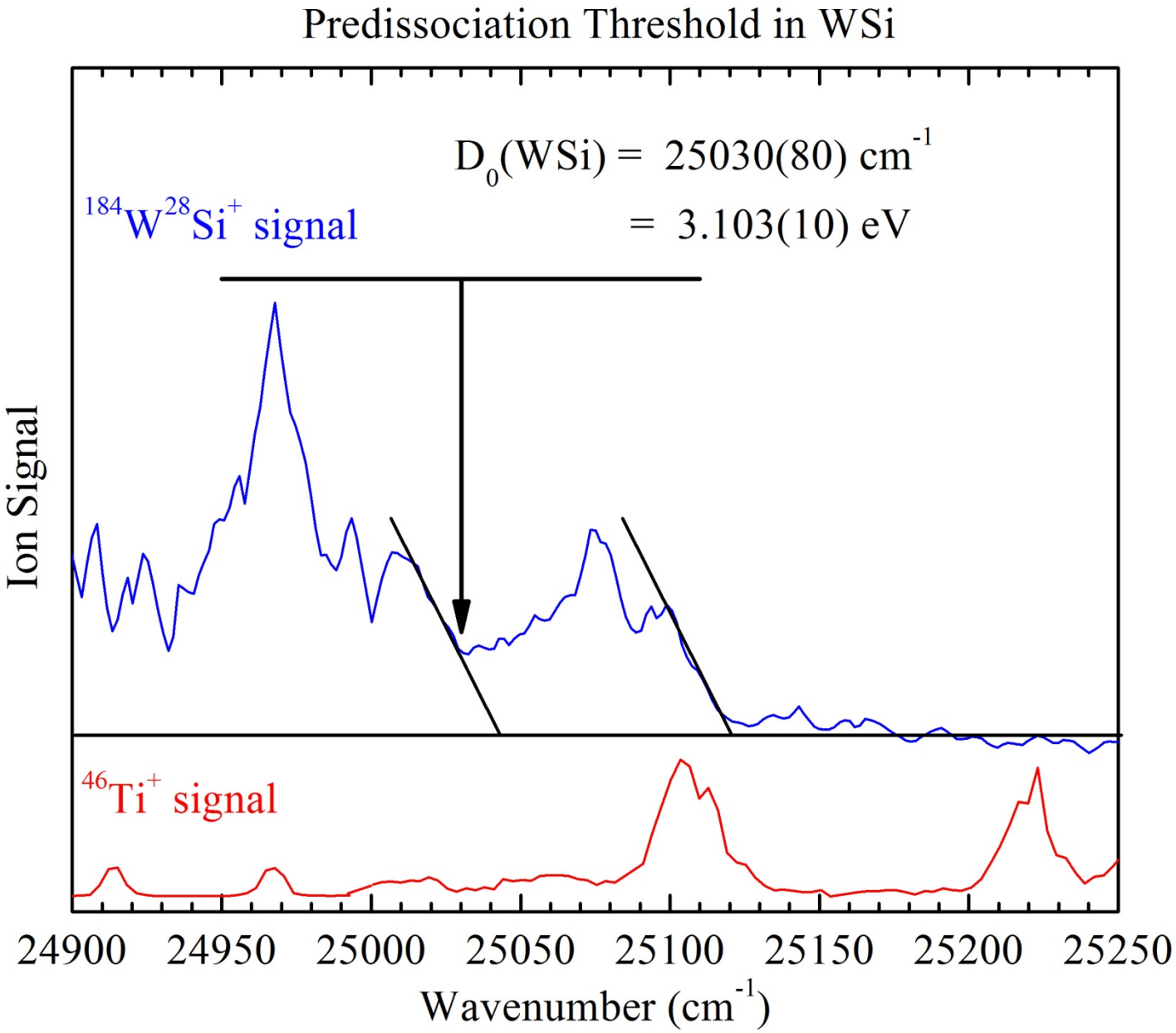

Figure 3. Expanded view of the predissociation threshold in tungsten silicide (WSi), showing the features that are interpreted as predissociation to the ground and first excited separated atom limits. Again, the horizontal bar at the top of the arrow indicates the ±80 cm^{-1} assigned uncertainty range. See text for details.

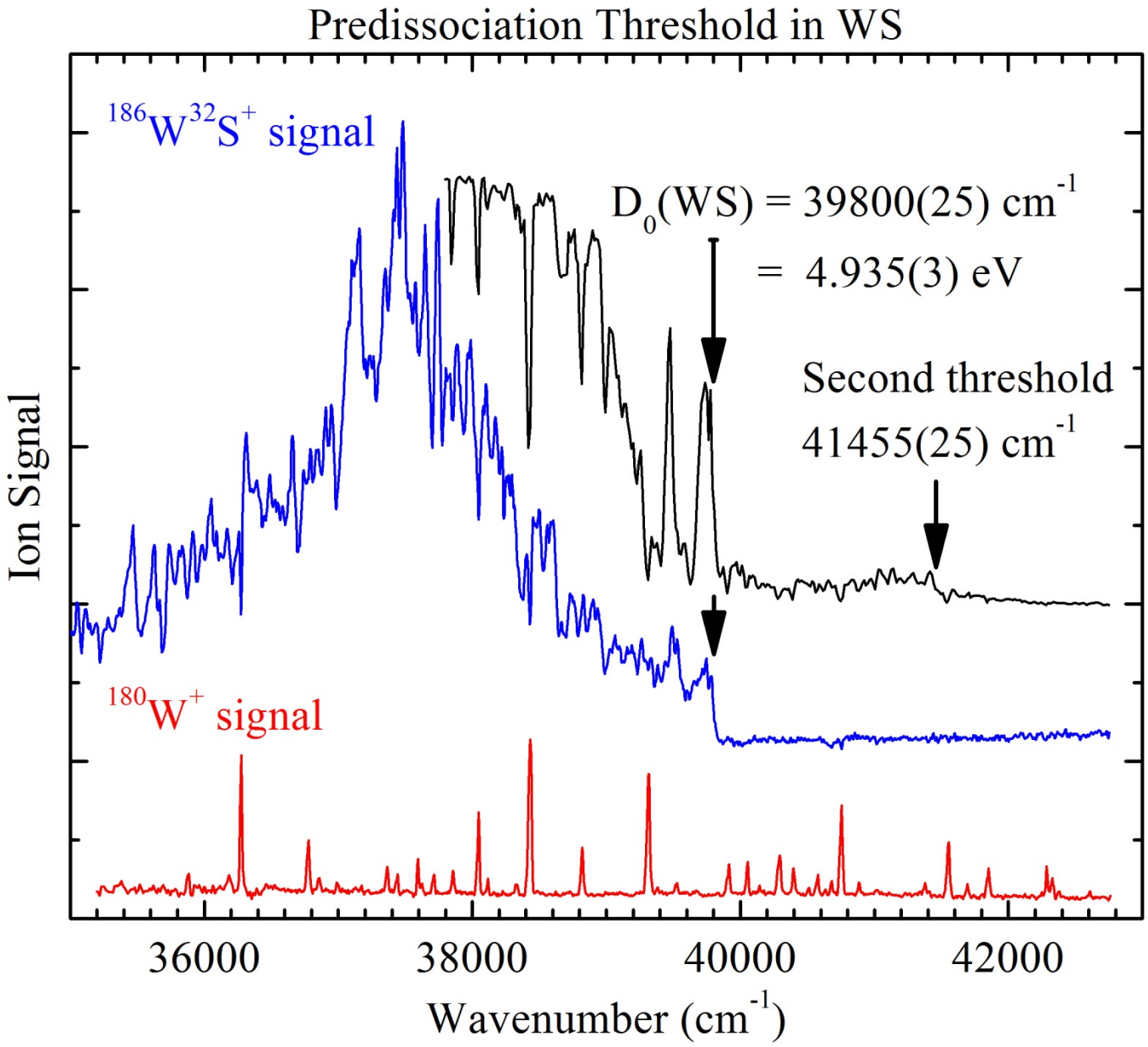

Figure 4. R2PI spectrum of tungsten sulfide (WS), showing the predissociation threshold at 39,800(50) cm^{-1}. The blue trace corresponds to ionization by an OPO + KrF process, with a 30 ns delay between excitation and ionization. The black trace corresponds to ionization by absorption of two OPO photons, with a delay between the two absorptions of less than 5 ns.

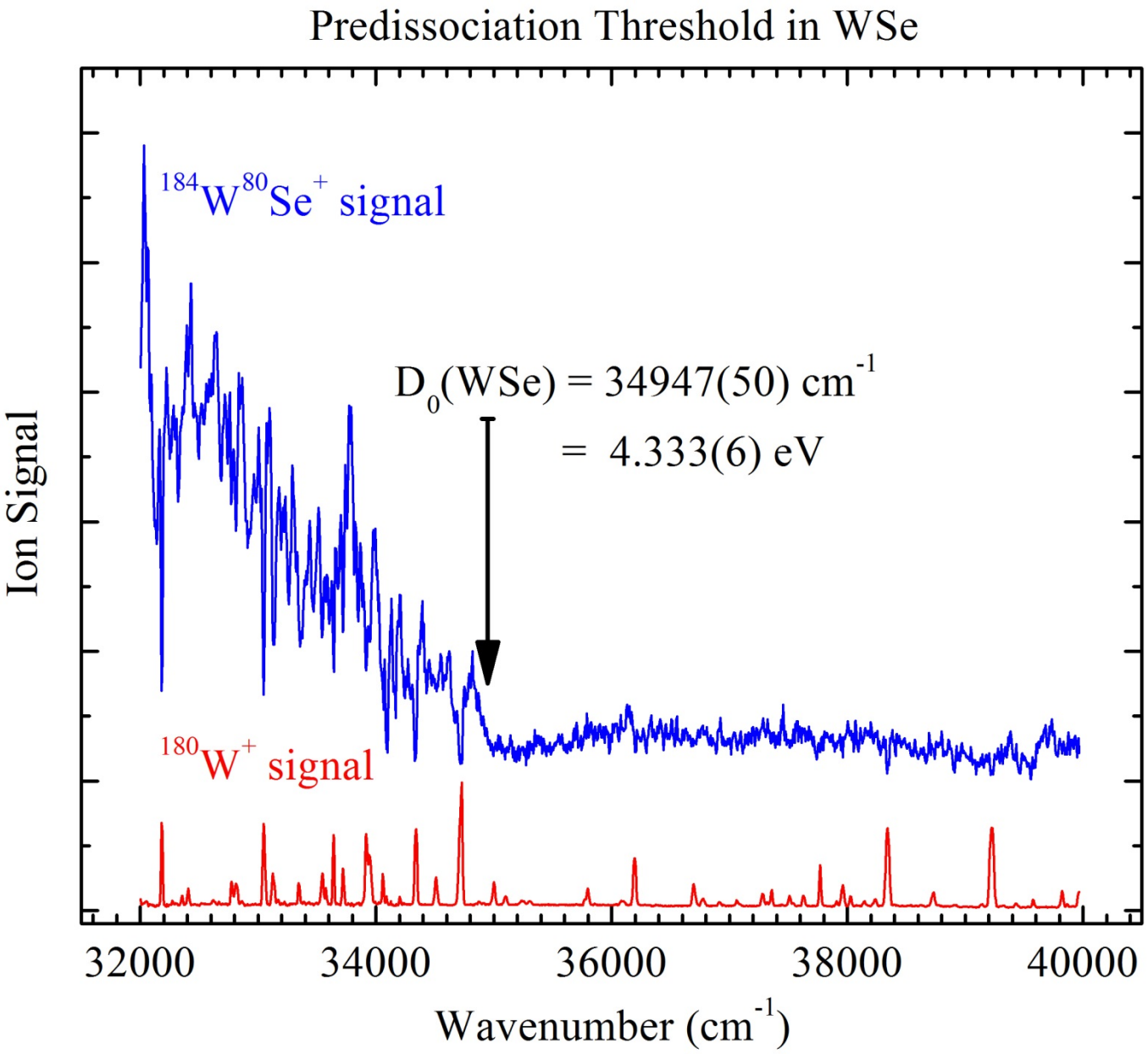

Figure 5. R2PI spectrum of tungsten selenide (WSe), showing the predissociation threshold at 34,947(50) cm^{-1}. The uncertainty range (±50 cm^{-1}) is indicated by the horizontal bar above the arrow showing the location of the predissociation threshold. Calibration was based on the atomic W transitions displayed in the lower trace.

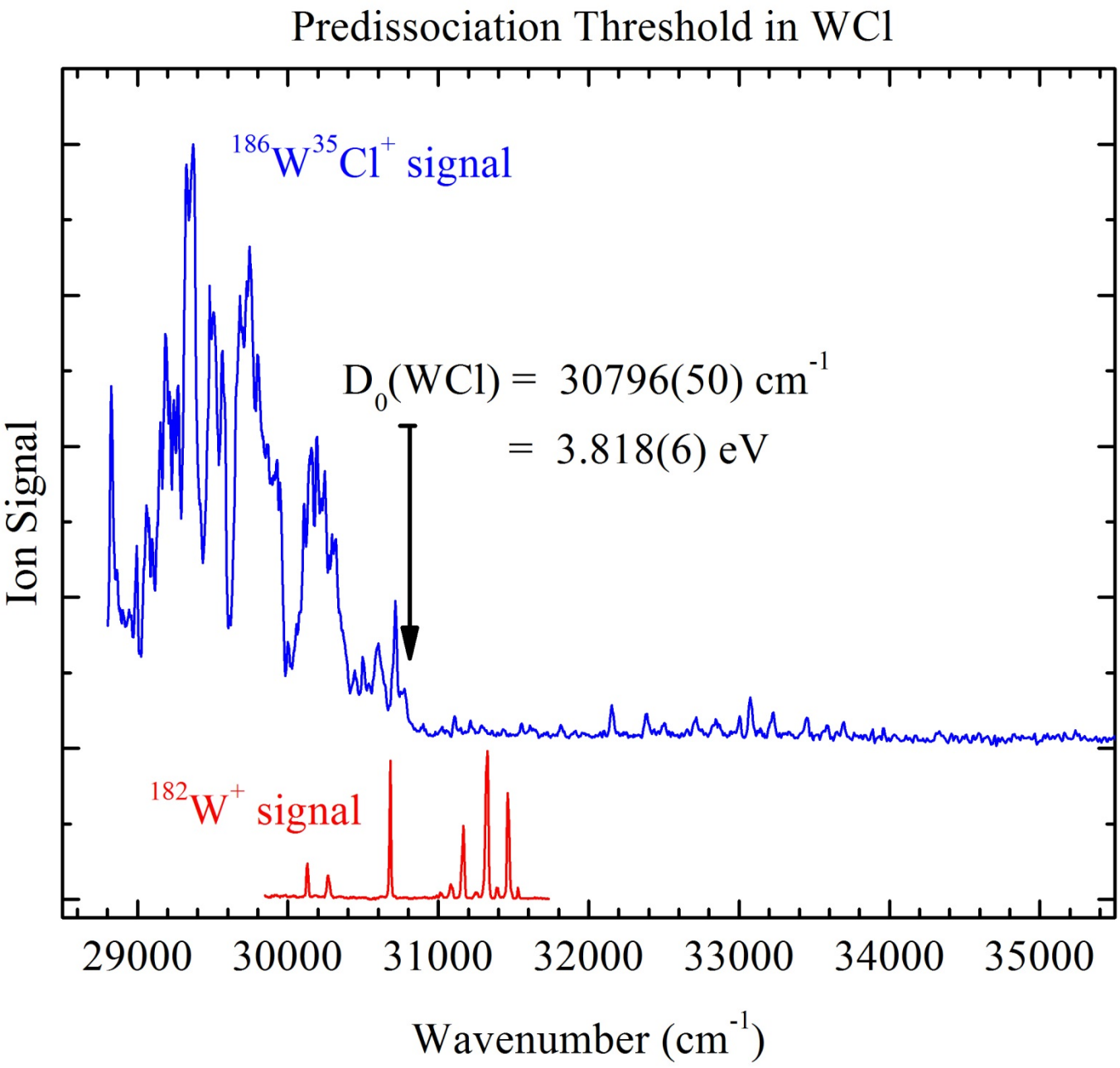

Figure 6. R2PI spectrum of tungsten chloride (WCl), showing the predissociation threshold at 30,796(80) cm^{-1}. The uncertainty range (±80 cm^{-1}) is indicated by the horizontal bar above the arrow showing the location of the predissociation threshold. Calibration was based on the atomic W transitions displayed in the lower trace.

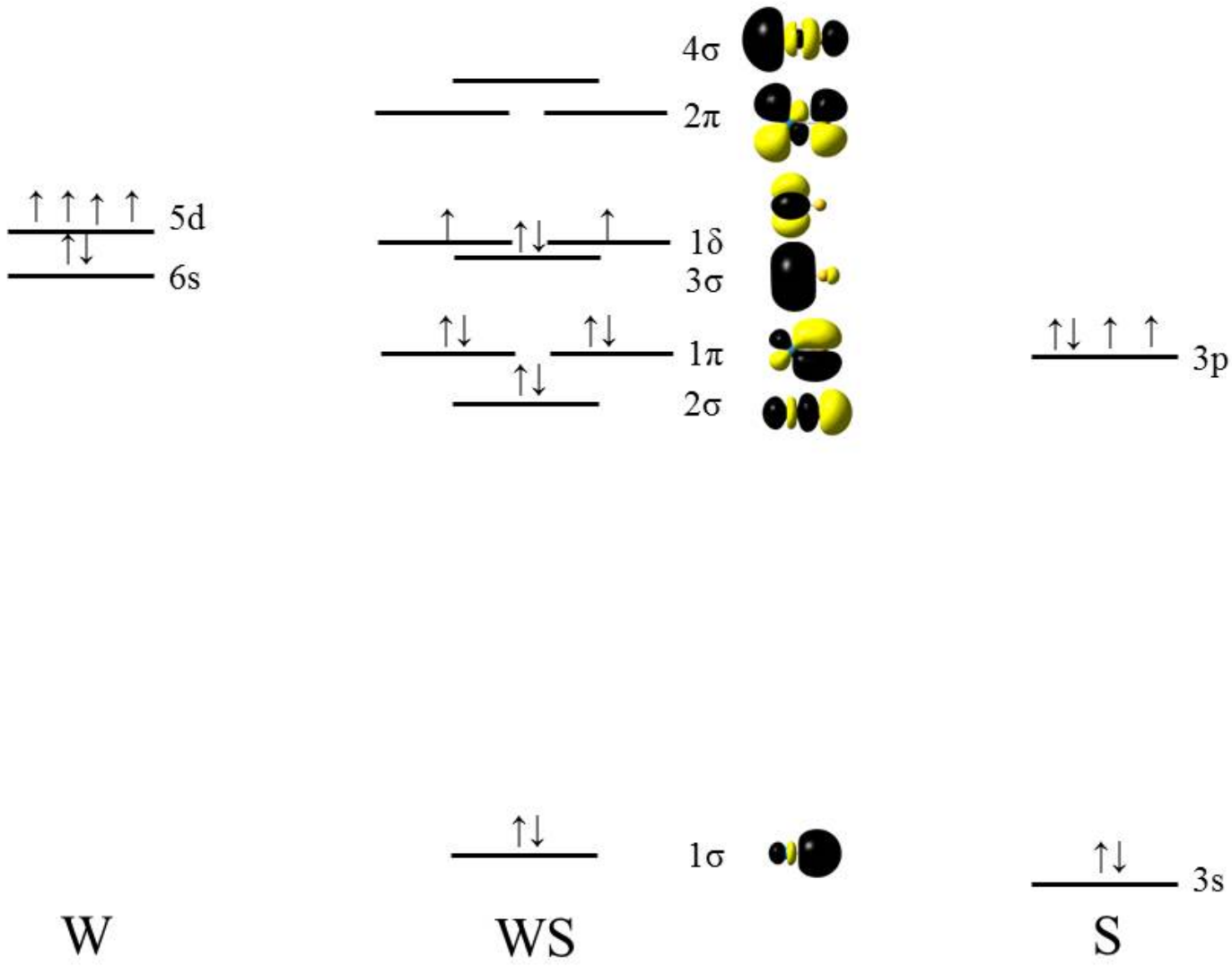

Figure 7. Molecular orbitals of the WX molecules, illustrated for WS.

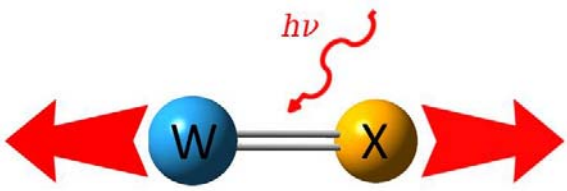

TOC Graphic